UNIVERSITY OF CALIFORNIA

Radiation Laboratory

BERKELEY, CALIFORNIA

UCRL-2975 Rev

UNIVERSITY OF CALIFORNIA

Radiation Laboratory
Berkeley, California

Contract No. W-7405-eng-48

EXPERIMENTS WITH 315-Mev POLARIZED PROTONS
I. ELASTIC SCATTERING BY COMPLEX NUCLEI

Owen Chamberlain, Emilio Segrè, Robert D. Tripp
Clyde Wiegand, and Tom Ypsilantis

February 1956

Printed for the U. S. Atomic Energy Commission

EXPERIMENTS WITH 315-Mev POLARIZED PROTONS
I. ELASTIC SCATTERING BY COMPLEX NUCLEI

Owen Chamberlain, Emilio Segrè, Robert D. Tripp,
Clyde Wiegand, and Tom Ypsilantis

Radiation Laboratory and Dept. of Physics
University of California, Berkeley, California

February 1956

ABSTRACT

In this paper we describe experiments with high-energy polarized protons, (~315 Mev), their production, and their scattering from complex nuclei. We give the essentials of the theory of polarization of particles of spin 1/2 in a form suitable to the interpretation of the experimental results. Included is a detailed description of the experimental techniques, the characteristics of the polarized beam, and a discussion of the errors of measurement. The beam was 76% polarized and the maximum beam current was approximately 10^5 protons per second. Results of the scattering experiments on beryllium, carbon, aluminum, calcium, iron, and tantalum are described. Some results of triple-scattering experiments, which further determine the scattering matrix, are also given. The relation to the experimental results of the various theories proposed for explaining the polarization by scattering is discussed. Only qualitative agreement with the theoretical studies made on current models is achieved. Although many of the features predicted by the usual type of potentials are present, no single potential can account for all the observed facts.

EXPERIMENTS WITH 315-Mev POLARIZED PROTONS
I. ELASTIC SCATTERING BY COMPLEX NUCLEI

Owen Chamberlain, Emilio Segrè, Robert D. Tripp,
Clyde Wiegand, and Tom Ypsilantis

Radiation Laboratory and Dept. of Physics
University of California, Berkeley, California

February 1956

INTRODUCTION

The polarization of beams of particles of spin 1/2 was first investigated in the celebrated Stern-Gerlach experiment. Mott[1] developed the theory of polarization for electrons and pointed out how polarization might be induced by scattering; many features of his work can be applied to proton beams. Polarized slow-neutron beams, obtained by scattering in ferromagnetic materials, have been known for some time, and the polarization of 2-Mev protons by resonance scattering from helium has been demonstrated by Heusinkveld and Freier,[2] following the analysis of Critchfield and Dodder.[3]

Wouters[4] attempted to polarize high-energy neutrons by collision in LiH and LiD, but could only demonstrate small effects due to polarization that were barely outside the observational errors. The first successful attempt to polarize high-energy protons was made by Oxley, Cartwright, Rouvina, Baskir, Klein, Ring, and Skillman[5] at the University of Rochester. Following the announcement of the Rochester results we initiated a series of experiments that have hitherto been reported only in brief communications.[6] This paper

---

1 N. F. Mott, Proc. Roy. Soc. (London) A 135, 429 (1932).

2 M. Heusinkveld and G. Freier, Phys. Rev. 85, 80 (1952).

3 C. L. Critchfield and D. C. Dodder, Phys. Rev. 76, 602 (1949).

4 L. F. Wouters, Phys. Rev. 84, 1069 (1951).

5 Oxley, Cartwright, Rouvina, Baskir, Klein, Ring, and Skillman, Phys. Rev. 91, 419 (1953). See also Oxley, Cartwright, and Rouvina, Phys. Rev. 93, 806 (1954).

6 Chamberlain, Segrè, Tripp, Wiegand, and Ypsilantis, Phys. Rev. 93, 1430 (1954); 95, 1105 (1954); 96, 807 (1954); 98, 266 (1955).

is a more complete description of the work, and is limited to the scattering of polarized protons by complex nuclei. Scattering by H and D are to be discussed in a subsequent paper.

Similar double-scattering experiments have been performed by Marshall, Marshall, de Carvalho, Heiberg, Kruse and Solmitz[7] at the University of Chicago; Dixon, Rose and Salter[8] in England; Kane, Stallwood, Sutton, Fields and Fox[9] at Carnegie Institute of Technology; and Strauch[10] at Harvard University and in this laboratory.

The theory of these experiments has been developed by many authors,[11-26] and we give here an outline of what is necessary in order to understand the experimental work. The Wolfenstein[21] notation is used throughout unless otherwise indicated.

---

7 Marshall, Marshall, and de Carvalho, Phys. Rev. 93, 1431 (1954); de Carvalho, Marshall, and Marshall, Phys. Rev. 96, 1081 (1954); and Heiberg, Kruse, Marshall, Marshall, and Solmitz, Phys. Rev. 97, 250 (1955).

8 J. M. Dixon and D. C. Salter, Nature 173, 946 (1954); and Dixon, Rose, and Salter, Proc. Phys. Soc. 68A, 361 (1955).

9 Kane, Stallwood, Sutton, Fields, and Fox, Phys. Rev. 95, 1694 (1954).

10 Karl Strauch, Phys. Rev. 99, 150 (1955); UCRL-3211, Nov. 1955.

11 L. Wolfenstein, Phys. Rev. 75, 1664 (1949).

12 J. V. Lepore, Phys. Rev. 79, 137 (1950). Equation (23) of this paper is in error. The sign of the $\underline{P}_{inc} \times \underline{n}$ term should be reversed.

13 E. Fermi, Nuovo Cimento 11, 407 (1954).

14 W. Heckrotte and J. V. Lepore, Phys. Rev. 94, 500 (1954).

15 Snow, Sternheimer, and Yang, Phys. Rev. 94, 1073 (1954).

16 B. J. Malenka, Phys. Rev. 95, 522 (1954).

17 I. I. Levintov, Doklady Akad. Nauk S.S.S.R. 98, 373 (1954).

18 E. Bosco and T. Regge, Nuovo Cimento 12, 285 (1954).

19 E. Clementel, Nuovo Cimento 1, 509 (1955).

20 R. Sternheimer. Phys. Rev. 95, 587 (1954); 97, 1314 (1955); 100, 886 (1955).

21 L. Wolfenstein, Phys. Rev. 96, 1654 (1954).

22 Fernbach, Heckrotte, and Lepore, Phys. Rev. 97, 1059 (1955).

23 R. Wilson, Phil. Mag. 46, 769 (1955)

24 T. Erikson, Nuovo Cimento 2, 911 (1955).

25 S. Kohler, Nuovo Cimento 2, 907 (1955).

26 A. Sjölander and S. Kohler, Arkiv. Fysik. 8, 521 (1954).

II. FUNDAMENTALS OF THEORY

A. Double-Scattering Experiments

In order to completely specify a beam of any kind of particles it is necessary to give its intensity, direction of propagation, and energy, and also its polarization. For particles of spin 1/2 the polarization may be represented by a vector

$$\underset{\sim}{P} = 2 \langle \underset{\sim}{s} \rangle , \tag{1}$$

where $\langle \underset{\sim}{s} \rangle$ is the expectation value of the spin in units of $\hbar$. The magnitude of $\underset{\sim}{P}$ varies between 0 and 1, the first value corresponding to an unpolarized beam, the second to a beam perfectly polarized. The direction of $\underset{\sim}{P}$ gives the "direction of polarization." The component of $\underset{\sim}{P}$ in a specified direction is equal to the ratio

$$P_z = \frac{N_+ - N_-}{N_+ + N_-} , \tag{2}$$

where N_+ and N_- are the numbers of particles with spin up or down that would be found; e.g., in a Stern-Gerlach experiment, with the inhomogeneity of H directed along z. The vector $\underset{\sim}{P}$ describes completely the polarization of particles of spin 1/2 and is equivalent to other complete descriptions such as that attainable by the use of a density matrix.[27]

The elastic scattering of a spin-1/2 particle from a spin-zero nucleus may be described through the use of a 2 x 2 matrix M, which when applied to the spinor, describing the incident beam, transforms it to the spinor of the scattered beam. The most general form of M has been deduced by Wolfenstein,[11] and also by Lepore,[12] as

$$M = g(\Theta) I + h(\Theta) \underset{\sim}{\sigma} \cdot \underset{\sim}{n}, \tag{3}$$

---

[27] L. Wolfenstein and J. Ashkin, Phys. Rev. 85, 947 (1952). See also R. H. Dalitz, Proc. Phys. Soc. 65A, 175 (1952).

where Θ is the laboratory scattering angle, I is the unit 2 x 2 matrix, $\underset{\sim}{\sigma}$ is the Pauli spin matrix. A unit vector $\underset{\sim}{n}$ perpendicular to the scattering plane is defined by

$$\underset{\sim}{n} = \frac{\underset{\sim}{k} \times \underset{\sim}{k'}}{|\underset{\sim}{k} \times \underset{\sim}{k'}|} \quad , \tag{4}$$

where $\underset{\sim}{k}$, $\underset{\sim}{k'}$ are the propagation vectors of the incident and scattered wave respectively. Here $g(\Theta)$ and $h(\Theta)$ are arbitrary complex functions of the scattering angle Θ and also of the energy of the incident particle. In elastic scattering of a beam of unpolarized nucleons by a spin-zero nucleus the vector $\underset{\sim}{P}$, for reasons of symmetry, is perpendicular to the plane of scattering, and its magnitude is given by

$$P = \frac{g^*h + gh^*}{|g|^2 + |h|^2} \quad . \tag{5}$$

The experimental determination of M was one of the objects of our work and is discussed later in more detail. The first step was the determination of $\underset{\sim}{P}$ for a given beam. The beam of the 184-inch Berkeley cyclotron was brought out of the vacuum chamber into the experimental area (cave) by scattering it on Target 1, deflecting it in a steering magnet, and bringing it out through the shielding as indicated in Fig. 1. Assuming, as we have checked experimentally, that the primary beam was unpolarized, the beam after the scattering by Target 1 was polarized with $\underset{\sim}{P}$ vertical. In order to detect this polarization an analyzer was needed, and we used a second scattering process at Target 2. It can be shown that if the incident beam has a polarization P_1, the differential-scattering cross section is given by

$$\begin{aligned} I(\Theta) &= \left(|g|^2 + |h|^2\right) \left(1 + \frac{g^*h + gh^*}{|g|^2 + |h|^2} \; \underset{\sim}{P}_1 \cdot \underset{\sim}{n}_2\right) = \\ I_0(\Theta) &\left[1 + \underset{\sim}{P}_1 \cdot \underset{\sim}{P}_2\right] = I_0(\Theta) \left[1 + P_1 P_2 \cos \Phi\right], \end{aligned} \tag{6}$$

where $\underset{\sim}{n}_2$ is defined by Eq. (4), but referred to the second scatterer.

If we scatter at angle O_2 and measure the relative intensities $I(\Phi = 0^\circ)$ and $I(\phi = 180^\circ)$ where ϕ is the azimuthal angle,[28] Eq. (6) gives

$$e = \frac{I(\phi = 0^\circ) - I(\phi = 180^\circ)}{I(\phi = 0^\circ) + I(\phi = 180^\circ)} = P_1 P_2, \tag{7}$$

where P_1 and P_2 are the polarizations that would be generated in the first and second scattering process respectively if one started in each case with an unpolarized beam.

If the two scattering processes at Targets 1 and 2 are identical, we have

$$P = P_1 = P_2 = \pm e^{1/2}. \tag{8}$$

The ambiguity in sign reflects the fact that an experiment of this type gives only the magnitude of $\underset{\sim}{P}_1$ without telling whether it points "up" or "down."

Thus far the discussion has been limited to scattering by a force center without spin. Actually, Eq. (8) may be shown to hold also for two successive identical scattering processes even if the target nuclei have a finite spin, providing that the targets are unpolarized and the scattering process is elastic. For the scattering on targets with spin we must consider elastic scattering processes of two kinds: those in which the incident particle suffers a spin flip—that is, the component of spin in the direction of the normal $\underset{\sim}{n}$ to the scattering plane is changed—and those in which there is no spin flip of the incident particle.

---

[28] Our coordinate system in the laboratory may be completely described as follows: The beam incident on the second target (Target 2) is moving in the positive z direction. The (horizontal) plane of the cyclotron orbit (and the plane of scattering at the first target) is the xz plane. The y axis is upward, thus the axes xyz form a right-handed coordinate system. Θ and Φ are the usual spherical coordinates, therefore $z = r \cos \Theta$, $x = r \sin \Theta \cos \Phi$, $y = r \sin \Theta \sin \Phi$. The scattering angles θ, ϕ in the center-of-mass system are related to the laboratory angles Θ, Φ through the usual transformations.

Let us indicate by $p(+L+)$ the probability that an incident particle with spin up will be scattered to the left with spin up and by $p(+L-)$ the probability that the particle will be scattered to the left with spin down. We have, all together, eight similar probabilities to consider, among which are the relations

$$\begin{aligned} p(+L+) &= p(-R-), \\ p(+L-) &= p(-R+), \\ p(-L+) &= p(+R-), \\ p(-L-) &= p(+R+). \end{aligned} \tag{9}$$

These relations are confirmed by remarking that if we rotate our reference system by $\Phi = \pi$ around the direction of the incident beam $p(+L+)$ goes into $p(-R-)$, etc.

If we start with an unpolarized beam and—using the $p(+L+)$, etc.—calculate the asymmetry e after a double-scattering experiment from identical targets, we find

$$e = P_1 \left\{ P_1 + \frac{2\,[p(+L-) - p(-L+)]}{p(+L+) + p(-L+) + p(+L-) + p(-L-)} \right\}, \tag{10}$$

where P_1 is the polarization after the first scattering in the beam scattered to the left. In order that Eq. (10) reduce to Eq. (8) we must have

$$p(+L-) = p(-L+), \tag{11}$$

and this occurs if the collision process is time-reversible, which in practice means elastic.

In order for Eq. (8) to be applicable the last condition is essential, and it can be fulfilled if we are sure that both scattering processes are elastic. However, we must neglect the small energy loss that is unavoidable because of recoil of the target nucleus and the energy losses due to ionization which the particles suffer in traversing the targets.

B. Triple-Scattering Experiments

In the elastic scattering of a particle of spin 1/2 from a spin-zero nucleus the most general scattering matrix is of the form of Eq. (3). This matrix contains four real independent parameters: the magnitude and phase of both g and h. Three of these parameters, i.e., $|g|$, $|h|$, and the phase difference β between $g + h$ and $g - h$, can be measured experimentally. The absolute phase of g and h could affect experimental results if it were possible to make waves from different nuclei interfere, as in slow-neutron coherent scattering, but it is not of importance in our experiments.

Wolfenstein[21] has shown that g and h are related to directly measurable quantities by

$$g + h = I_0^{1/2} (1 + P)^{1/2} e^{i\alpha}, \tag{12}$$

$$g - h = I_0^{1/2} (1 - P)^{1/2} e^{i(\alpha-\beta)}, \tag{13}$$

where I_0 is the differential scattering cross section for an unpolarized beam, P is the polarization, α is the unessential absolute phase (which in our case could be assumed to be zero), and β is the phase between $g + h$ and $g - h$.

We have obtained some measure of the quantity β by performing a triple-scattering experiment with a geometry shown in perspective in Fig. 2. The unpolarized cyclotron beam was first scattered in a horizontal plane π_1 from Target 1 through an angle Θ_1. This operation served only to produce a polarized beam with the polarization vector $\underset{\sim}{P}_1$ directed vertically. This polarized beam was scattered in the vertical plane π_2 from Target 2. The angle of scattering was Θ_2. The twice-scattered beam was subsequently scattered from Target 3 in the π_3 plane. The purpose of the last scattering was to analyze the twice-scattered beam; or, more precisely, to find the component of the vector $\langle \underset{\sim}{\sigma} \rangle_2$ in the direction perpendicular to the direction of propagation and contained in the plane π_3. This component is $\langle \underset{\sim}{\sigma} \rangle_2 \cdot \underset{\sim}{s}_2$, where $\underset{\sim}{s}_2 = \underset{\sim}{n}_2 \times \underset{\sim}{k'}_2$.

We will call e_{3s} the asymmetry corresponding to the scattering in Target 3, i.e., the ratio of the beam intensities $I_3(+) - I_3(-) / I_3(+) + I_3(-)$, where $I_3(\pm)$ refers to the scattering such that $\underset{\sim}{n}_3$ is parallel to $\pm\underset{\sim}{s}_2$. Wolfenstein[21] has defined the parameter R by the relation

$$R = \frac{e_{3s}(1 + P_1 P_2 \cos \Phi_2)}{P_1 P_3 \sin \Phi_2}, \tag{14}$$

where P_3 is the magnitude of the polarization vector obtainable in the elastic scattering of an unpolarized beam from Target 3. In our measurements we have $\Phi_2 = 270^\circ$, which corresponds to the third scattering angle in a downward direction, thus we get

$$R = -\frac{e_{3s}}{P_1 P_3}. \tag{15}$$

Now R is connected to β through the relation

$$R = (1 - P_2^2)^{1/2} \cos(\theta_2 - \beta), \tag{16}$$

where, as usual, P_2 is the magnitude of the polarization obtainable in the elastic scattering of an unpolarized beam from Target 2. From Eq. (16) it is apparent that a measurement of R gives $\cos(\theta_2 - \beta)$ and hence two possible values of β. This ambiguity is inherent in the method of measurement. The quantity β is susceptible to a simple geometrical interpretation: it is the angle by which the component of $\langle \underset{\sim}{\sigma} \rangle_2$ in the plane π_2 is rotated with respect to $\underset{\sim}{n}_1$.

Any specific theory of polarization gives, if complete, definite values for β, thus it should be possible to compare this prediction with the experimental results. In particular, for the case in which the polarization is caused by a potential as in Eqs. (24) and (25) specialized to a square well, Wolfenstein has calculated, in Born approximation, the values to be expected for e_{3s}.[29]

---

[29] L. Wolfenstein (private communication). In the text of Reference 21 several errors should be noted. In equations (2.5) and (2.6), β should be replaced by $(-\beta)$. In Table I the columns labeled β, e_{3s}, e_{3s}' should be relabeled as $-\beta$, e_{3s}', e_{3s} respectively.

There is another type of triple-scattering experiment in which all scatterings occur in the same plane. In this experiment the asymmetry e_{3n} after the third scattering is given by

$$e_{3n} = \frac{P_3 (P_2 + DP_1 \cos \bar{\Phi}_2)}{1 + P_1 P_2 \cos \bar{\Phi}_2} \quad . \tag{17}$$

Equation (17) defines a new parameter D, which depends on the particular interaction of Target 2. D measures the probability that the incoming polarized protons maintain their direction of spin on scattering. For the scattering of protons from a spin-zero nucleus, D is unity for all scattering angles.

III. THE POLARIZED BEAM

Calculations of proton trajectories in the cyclotron field indicated the approximate range of target positions within the cyclotron tank from which scattered protons might enter the evacuated external beam tube. An external beam was readily obtained when a target was placed approximately as shown in Fig. 1. Scattering measurements with second targets of beryllium and carbon indicated that the beam was highly polarized, and range measurements showed its energy to be 285 Mev, with an rms energy spread (standard deviation of a gaussian distribution of energies) of about 12 Mev. Once the energy was known better orbit calculations could be made, and it was determined that the scattering angle at the first target was 17°. A number of double-scattering experiments were performed with this beam. However, double elastic scattering experiments (with both targets of beryllium) indicated that the asymmetries were largest for second-scattering angles of about 13°. This meant that greater beam polarization could be achieved if the first scattering angle were near this value. Further orbit calculations indicated that this was indeed possible, and the placement of Target 1 shown in Fig. 1 was found satisfactory. For this position the first scattering angle Θ_1 has been calculated to be 13° for the observed energy, 315 Mev, of the polarized beam.

In all cases the steering-magnet current was adjusted to the highest value consistent with reasonable beam intensity, so that only the highest-energy

components of the scattered protons from the first target were utilized. Under these circumstances we were satisfying, as well as possible, the requirement that the polarized beam be made up only of elastically scattered protons, so that the beam polarization could be measured as previously outlined in connection with Eq. (8). Table I shows results of double-scattering experiments in which both targets were of beryllium, along with calculated values of the polarization. The beam energy E_1 was slightly different for different cyclotron runs.[30] Because highly inelastic scattering processes were completely rejected and the scattering angle was small enough so that elastic scattering strongly predominated over inelastic scattering, we believe we are justified in using Eq. (8). The datum of Table I for $\Theta_2 = 13^\circ$ was used together with Eq. (8) to determine the magnitude of the beam polarization as 0.76. Equation (7) was used, with $P_1 = 0.76$, to find the values of P at other angles.

The sign of the polarization has been determined by Marshall and Marshall[31] and Brinkworth and Rose,[32] and it is such that for a proton that is scattered to the left, the spin points upwards.

The intensity of the polarized proton beam was $5 \times 10^4 \frac{\text{protons}}{\text{cm}^2\text{-sec}}$. Two different beam exit apertures were utilized. In the elastic double-scattering measurements, where energy resolution was of primary importance, the aperture used was 2 in. vertical by 0.5 in. horizontal, corresponding to an area of 6.45 cm^2. The polarized proton beam energy was measured by determining the Bragg curve. Two ionization chambers and a variable copper absorber were used as described in Reference 33. The beam energy (with rms energy spread) was 315 ± 5 Mev. In the triple-scattering measurements a

---

30 The absorber in the detecting telescope was adjusted in such a way as to accept protons that has lost up to 12 Mev of energy in inelastic collisions, in addition to the unavoidable energy losses due to elastic recoil of the target nucleus and ionization losses in traversing the target.

31 J. Marshall and L. Marshall, Phys. Rev. 98, 1398 (1955).

32 Brinkworth and Rose, Fifth Annual Rochester Conference on High-Energy Nuclear Physics, Interscience, 1955.

Table I

Double scattering from beryllium; $\Theta_1 = 13^\circ$

Θ_2	E_1(Mev)	e	I_0 $10^{-27}\frac{cm^2}{steradian}$	P_{Be}
10°	312 ± 4	0.512 ± 0.022	146.2 ± 2.0	0.673 ± 0.029
13°	318 ± 5	0.580 ± 0.010	71.0 ± 1.2	0.761 ± 0.007
15°	318 ± 5	0.555 ± 0.015	44.2 ± 1.0	0.730 ± 0.020
15°	312 ± 4	0.534 ± 0.022	45.4 ± 1.2	0.701 ± 0.029
17°	318 ± 5	0.476 ± 0.025	27.2 ± 0.7	0.626 ± 0.033
19°	318 ± 5	0.394 ± 0.023	19.1 ± 0.5	0.518 ± 0.030

circular exit aperture, 2 in. in diameter, was used in order to increase the beam current. The measured energy and rms energy spread of this beam was 315 ± 12 Mev.

The duty cycle of the polarized beam appears to be considerably greater than that of the unpolarized external beam. Accidental-coincidence-rate studies show that there are effectively about 80,000 cyclotron radio-frequency pulses per second during which the protons are emitted. Each of these pulses lasts about 10^{-8} sec; they come in trains of about 1300 pulses, the whole train of pulses lasting about 80 microseconds. There are 60 of these pulse trains per second. With our coincidence resolving power we do not resolve two protons coming in the same rf pulse.

IV. EXPERIMENTAL TECHNIQUE

A. Double Scattering

The beam intensity was determined with argon-filled ionization chambers, by the same techniques and apparatus as described in a previous publication.[33]

The scattering table, upon which the counters were mounted, consisted of a rigidly constructed frame which allowed the polar and azimuthal scattering angles to be varied independently. This frame rotated about two large hollow bearings and was counterweighted to minimize distortions due to the weight of the apparatus. The position of the counter telescope with respect to the beam was checked by a surveyor's transit as a function of the azimuthal orientation Φ_2. The rigidity of the frame was such that the counter telescope was symmetrically located with respect to the beam to better than 0.06°. The settings of the scattering angle Θ_2 were accurate to 0.1°; however, errors in the setting of Θ_2 did not contribute to the error in the measurement of asymmetries. This is apparent from the fact that the asymmetries were obtained by comparing intensities at $\Phi_2 = 0^\circ$ and $\Phi_2 = 180^\circ$ for the same Θ_2 setting.

---

[33] Chamberlain, Segrè, and Wiegand, Phys. Rev. 83, 923 (1951).

The targets used were solid slabs of material or liquid helium. The liquid helium container was slightly modified from one originally designed for use with liquid hydrogen.[34] (Target thicknesses are described along with the summary of the experimental results.)

In the double-scattering measurements the protons scattered from Target 2 through angle Θ_2 were detected by a three-counter telescope shown in Fig. 3. Each counter consisted of a polished plastic scintillator viewed from the top and bottom by magnetically shielded 1P21 photomultiplier tubes.

The associated electronic circuits were quite conventional and had resolving times of approximately 10^{-8} sec. Before each data-taking session the electronic system was adjusted to be on a plateau of the curve of photomultiplier voltage (sensitivity) versus coincidence counting rate. The time resolution of the system was checked by taking curves of counting rate versus delay time between counters.

The alignment of the beam was determined by exposing x-ray films near the front and rear of the scattering apparatus. With the aid of the transit the center of rotation of the scattering table could be placed along the beam center to an accuracy of about 0.03 in. at the front film and 0.05 in. at the rear film. In this process the correct alignment of the table was achieved to 0.06°.

In the later experiments the photographic alignment procedure was supplemented by a more precise electronic alignment. The counter telescope was moved to a very small polar angle Θ_2 and the counting rate due to multiple scattering in the target was measured at 0° and 180° azimuthal angles Φ_2. In this region the counting rate is an extremely sensitive function of the scattering angle Θ_2, changing by a factor of 10 for 1° change in the angle. Small readjustments of the rear of the scattering table were made to equalize the counting rates at $\Phi_2 = 0^\circ$ and 180°; the alignment was then believed to be accurate to 0.02°. This precision was sufficient to make the errors in polarization due to misalignment no larger than 0.03, even for the heaviest elements studied.

---

[34] J. W. Mather and E. A. Martinelli, Phys. Rev. 92, 785 (1952).

The 15-gauss magnetic field existing in the experimental area could give rise to a misalignment of 0.02° in the photographic alignment procedure, because the spacing of the x-ray films was not the same as that between target and counter telescope. The electronic alignment procedure was not subject to error due to the magnetic field.

The range of the protons in the beam was determined with the counter telescope by measuring the number of counts per unit incident beam as a function of the thickness of absorber placed in the counter telescope. The data are plotted in the form of a curve, with number of counts as ordinate and energy cutoff as abscissa. If there were no nuclear absorption and only elastic scattering such a curve would look almost rectangular. The nuclear absorption and inelastic scattering give a slope to the flat part and the results are curves of the type shown in Fig. 4. The variation in slope as a function of the scattering angle arises because the ratio between elastically and inelastically scattered particles decreases rapidly with increasing Θ_2. For scattering angles $\Theta_2 > 0.61 \frac{\lambda}{R}$ (where λ is the de Broglie wave length of the incident proton and R is the radius of the struck nucleus) the scattering is largely inelastic and the spectrum of the scattered protons is almost a continuum. Range curves at these angles do not show the abrupt change in slope near the end of the range that characterizes the range curves shown in Fig. 4.

The energy resolution of the counter telescope was, in principle, limited only by the range straggling in the absorber; however, the most important contribution to the energy resolution of this system was due to the energy spread of the polarized beam. The rms energy width due to both of these effects was approximately ± 6 Mev. For most of the elements studied the levels of nuclear excitation, of the order of 1 Mev, could not be resolved with this system. An exception to this situation was in helium, which has no excited levels. Dissociation of the helium nucleus requires 20 Mev, thus the elastic events could be resolved by counting only those protons which had lost less than 20 Mev in the scattering.

The energy (or range) cutoff value was chosen well inside the knee of the range curve (see Fig. 4). One might have hoped to operate beyond the knee in order to most effectively separate the elastic from the inelastic components of the scattering. In this region, however, the counting rate was a very sensitive function of energy, consequently small time variations in the incident-beam energy would produce significant changes in the counting rate. A second

argument against operating at an energy higher than that of the knee of the range curve is the nonuniform energy profile of the polarized beam. The momentum analysis of the beam in the cyclotron fringing field and steering magnet introduces an energy variation of 2.5 Mev per inch in the horizontal plane at the position of the last collimator. If the energy cutoff were chosen beyond the knee, then the low-energy side of the beam entering the cave would be rejected, thus displacing the center of gravity of the beam toward the high-energy side. This, in effect, would produce a misalignment of the apparatus, which could result in large false asymmetries because of the strong dependence of the elastic cross section upon the scattering angle. This effect was minimized by the use of the 0.5-inch horizontal collimator and by choosing the energy cutoff in a region where the counting rate was an insensitive function of the energy cutoff, i.e, inside the knee of the range curve. For scattering angles $\Theta_2 \lesssim 0.61 \frac{\lambda}{R}$ this choice was always possible. For larger scattering angles the range curves obtained did not show the characteristic knee near the end of the range because of the increasing importance of the inelastic scattering. At these angles, however, the measured differential cross section was a relatively slowly varying function of the scattering angle; thus we believe our final results are not adverseley affected by the energy variation across the beam. In some of the published work of others, however, there area few results that may be somewhat in error because of this effect, which simulates a rapid variation of the polarization with change of the absorber thickness towards the end of the range of the scattered particles. In general the choice of the energy cutoff was made at very small scattering angles (0° to 5°). As the angle of scattering was increased the energy cutoff value was corrected to the nearest 1/4 Mev, to take into account the increased target thickness and recoil energy of the target nucleus.

Many of the theoretical predictions for polarization and elastic scattering call for narrow angular regions in which the polarization fluctuates rapidly near the angles of minima of the diffraction scattering. This suggests that the experiments should be performed with as good angular resolution as possible consistent with adequate counting rates. With the available polarized beam an angular resolution of about 1° has appeared to be a good compromise

between angular resolution and intensity. The geometrical factors entering into the angular resolution are the beam size, counter size, and divergence of the beam. For our most common experimental arrangement the fold of these three factors can be approximated by a gaussian shape of rms deviation 0.62°. For the helium target there was a further impairment of the resolution due to the finite thickness of the target in the direction of the beam. The angular resolution is also affected by the multiple scattering in the target. In most cases this has been made about equal to the angular resolution width due to geometrical effects. In some cases the calculated angular resolution has been compared with the angular resolution determined experimentally by sweeping the counter telescope through the beam. The two widths have in all cases agreed to within 10%. The angular resolutions in the double-scattering measurements are summarized in Table II.

The measurement of e is subject to errors, which originate from the usual statistical errors and from alignment errors. The error due to angular misalignment is given approximately by the relation (valid when $e^2 \ll 1$)

$$\Delta e = \frac{d \log I_0}{d\theta} \quad \Delta \Theta, \tag{18}$$

where Δe and $\Delta \Theta$ are the errors in e and Θ. The importance of this cause of error is shown in Table III, where we list the maximum value of $d \log I_0/d\Theta$ and the resulting uncertainty in polarization due to misalignment.

In order to check the general operation of our system against a theoretical prediction about which there is no doubt, we measured the intensity of the scattered beam (at constant Θ_2) as a function of the azimuthal angle ϕ_2. This intensity must be of the form

$$I(\Theta_2, \phi_2) = I_0(\Theta_2)\left[1 + e \cos \phi_2\right]. \tag{19}$$

Figure 5 shows the result of this measurement.

It was important to determine the state of polarization of the normal external beams of the cyclotron, which were obtained by electric deflection or by scattering through a very small angle. Many measurements have been made

Table II

Angular resolution in double scattering

Element	Target Thickness (g/cm^2)	Calculated multiple-scattering rms resolution (degrees)	Calculated total rms resolution (degrees)	Measured total rms resolution (degrees)
Be	2.1	0.27	0.68	-
C	3.2	0.45	0.77	0.84
Al	5.0	0.87	1.08	-
Ca	3.8	0.76	0.99	-
Fe	2.6	0.72	0.96	1.00
Ta	1.3	0.69	0.93	-

Table III

Maximum polarization errors due to angular misalignment

Element	$\left(\frac{d \ln I_0}{d\theta}\right)\left(\text{deg}^{-1}\right)$ Max	$\Delta\theta$ (degrees)	ΔP
He	0.22	0.15	0.043
Be	0.25	0.02	0.007
C	0.33	0.06	0.026
Al	0.40	0.06	0.032
Ca	0.65	0.06	0.051
Fe	0.70	0.02	0.018
Ta	1.00	0.02	0.026

with such beams in the past and the results were always interpreted under the tacit assumption that the beam was not polarized. A direct experiment proved the correctness of this assumption.

B. Coulomb Interference Effects in Double Scattering

The angular interval where interference effects between the Coulomb and nuclear elastic scattering might be expected can be estimated in the following manner. The Coulomb differential-scattering cross section for relativistic protons scattered from a nucleus having charge Z uniformly distributed throughout a sphere of radius R has been given by Gatha and Riddell[35] as

$$I_0^{\,c} \left(\frac{Ze^2}{2W\beta^2} \right)^2 \sin^{-4} \frac{\theta}{2} \left[1 + \left(kR \sin \frac{\theta}{2} \right)^2 \right] \qquad (20)$$

where θ is the center-of-mass scattering angle, W is the total energy, and $\hbar k$ is the momentum and β the velocity divided by c of the incident proton. The nuclear scattering at small angles from a complex square well in the Born approximation is given by Fernbach, Heckrotte, and Lepore[22] as

$$I_0^{\,N} = \left(\frac{2M}{\hbar} \right)^2 |u + iw|^2 \, R^6 \left\{ \frac{j_1 (2kR \sin \theta/2)}{2kR \sin \theta/2} \right\}^2 \qquad (21)$$

where u and w are the real and imaginary well depth and j_1 is the spherical Bessel function. Since the angular dependence of the nuclear scattering at small angles (i.e., $\sin \theta = \theta$) is determined by the diffraction character of the scattering, the specific model chosen for the calculation is of little consequence. The maximum interference effects should be expected when $I_0^{\,c} \cong I_0^{\,N}$, which occurs when $\theta = \theta_0 \cong 1/kR$. Experiments designed to observe the interference in the polarization and cross section have been carried out with targets of C, Fe, and Ta. The corresponding values of θ_0 for these elements are 4.1°, 3.3°, and 2.7°, respectively.

---

[35] K. M. Gatha and R. J. Riddell, Jr., Phys. Rev. 86, 1035 (1952).

In order to measure the polarization and cross section at these small angles it was necessary to improve the angular resolution of the system described in the preceding section. The counter telescope used for these measurements was similar to that shown in Fig. 3 except that the dimensions of the counters, in the order traversed, were 0.5 by 2 by 0.25 inches, 2 by 6 by 0.25 inches, and 2.5 by 8 by 0.38 inches. The distance between the first counter and the target was 50 inches, thus the solid angle subtended was 10^{-4} steradian. For this particular arrangement the geometrical factors entering into the angular resolution lead to an approximately gaussian resolution function with rms deviation of 0.23°. The contribution to the resolution function due to multiple scattering in the targets is summarized in Table IV.

The remainder of the experimental arrangement was identical in all respects with that described in Section IVA. The errors due to angular misalignment are somewhat larger in the small-angle measurements because of the more rapid variation of the average differential cross section in the region where Coulomb scattering becomes important. The maximum systematic errors from the source can be obtained through the use of Eq. (18). These are summarized in Table V.

C. Triple Scattering

The principal problem in triple-scattering experiments, where the second and third scatterings were done in the same experimental area, was to obtain a significant counting rate from the third target in the presence of a large background from the second target. Sacrifices in angular and energy resolution beyond those made in double-scattering experiments were necessary in order to achieve a feasible experiment. The counting rate obtained was from 1 to 10 counts per minute, depending on the elastic cross section of the second target in the angular region under investigation. Alignment and various checks were performed, and statistically significant data were obtained, at the rate of about 1 angle per day. The background problem from the second target was surmounted by electronically defining, with a pair of counters, a beam

Table IV

Angular resolution in small-angle double scattering

Element	Target Thickness (g/cm^2)	Calculated multiple-scattering rms resolution (degrees)	Calculated total rms resolution (degrees)	Measured total rms resolution (degrees)
C	1.00	0.24	0.34	0.35
Fe	0.48	0.31	0.38	0.42
Ta	0.27	0.33	0.41	0.46

Table V

Maximum polarization errors due to angular misalignment in small-angle double scattering

Element	$\left(\frac{d \ln I_0}{d\Theta}\right)_{Max} \left(deg^{-1}\right)$	$\Delta\Theta$ (degrees)	$\Delta\theta$
C	1.27	0.02	0.033
Fe	3.34	0.02	0.088
Ta	1.33	0.02	0.035

scattered from the second target at the angle of interest. This beam was then scattered by a third target into a proton telescope placed in coincidence with the defining counters. The multiple coincidence therefore defines a trajectory which permits only protons scattered from the third target to be recorded.

The full-intensity polarized beam was obtained by the use of a collimator 2 inches in diameter, and the resulting beam current (impinging on the second target) was 10^6 protons/sec with an energy of 315 ± 12 Mev.

The second target consisted of about 10 g cm^{-2} of aluminum or carbon. The second-scattered beam was defined by a pair of plastic scintillators, 3 by 3 by 0.25 inches, placed in line 20 inches and 40 inches from the second target. This resulted in a geometrical resolution of 1.5° and an rms projected multiple-scattering angle of about 1° for the aluminum target.

Immediately behind the second defining counter was the third scatterer (or analyzer), which measured the change in proton spin induced by the second scattering. The choice of the analyzer was dictated by two considerations: it must give a large polarization in an angular region where the elastic-scattering cross section is large, and it must have a low atomic number to reduce multiple scattering. A beryllium target was found suitable. The thickness of 10.5 g/cm^2 represents the maximum thickness commensurate with the small multiple scattering demanded by the geometry of the third scattering.

The third-scattered beam was detected by a counter telescope similar to the one used for double scattering. The counters, however, were larger; their dimensions, in the order traversed, were 2.5 by 8 by 3/8 inches; 3 by 9 by 3/8 inches; 4 by 10 by 3/8 inches. The distance from the center of Target 3 to the front counter of the telescope was 20 inches.

Since only elastically scattered protons from the second target were under investigation, the proton telescope had to contain absorbers, as in double scattering, in order to reject inelastic protons. The energy cutoff was set by placing the apparatus directly in the incident polarized beam, with the second and third targets in place and all counters in line (i.e., $\Theta_2 = 0^\circ$, $\Theta_3 = 0^\circ$). A range curve similar to those shown in Fig. 4 was obtained with the beam reduced to a low level and the 1-2 counters used as a monitor.

This curve was utilized in choosing the absorber thickness, as described for the double-scattering measurements. Suitable corrections were made for energy loss due to recoil and increased target thickness when $\Theta_2 \neq 0^\circ$ and $\Theta_3 \neq 0^\circ$.

The alignment for triple scattering requires some comment. There was no special alignment problem at the second target, but at the third target great care was required to insure that the left and right scattering angles Θ_3 were equal. For the D experiment the second and third scattering planes coincide. The rapidly varying elastic cross section from the second target causes an extremely nonuniform illumination of the third target; the intensity of elastic protons scattered from aluminum at a mean angle $\Theta_2 = 12^\circ$ changes by a factor of eight across the third target. This is true for both the D and R geometry. In the latter measurements, however, the third scattering plane is normal to the second scattering plane, thus the nonuniform illumination of the third target could not induce false asymmetries. We have used the counter telescope consisting of Counters 3, 4 and 5 (in coincidence with Counters 1 and 2, which define the second-scattered beam) to determine the effective zero angle for Θ_3. Counting (1-2-3-4-5) rates were measured for many settings of the angle Θ_3 near zero angle so that a profile curve of the twice-scattered beam could be drawn. To a first approximation the centroid constitutes the proper zero of angle for Θ_3. This is quite adequate for the measurement of R. For the measurement of D, where the intensity asymmetry is more serious, a slightly more elaborate procedure has been used which takes into account the known angular dependence of the scattering on the beryllium of the third target. Since the beam-profile curve was determined with the same absorber thicknesses in the 3-4-5 telescope as were used in the actual measurements, we feel that this curve does determine satisfactorily the effective center of the second-scattered beam. The experiment to determine D for carbon, which is of necessity unity since the spin of carbon is zero, was conceived as a severe test of the alignment method, and the measured D value indicates no statistically significant departure from the anticipated result.

The calibration of the analyzer, i.e., the determination of P_3, was achieved by an independent measurement. The quantity that was actually measured was the product $P_1 P_3$ at the energy corresponding to the energy of the twice-scattered beam. This was accomplished by setting $\Theta_2 = 0$ and

replacing Target 2 with a uranium target of the same stopping power. The protons of the polarized beam were multiply scattered by the uranium to such an extent that the 1-2 counters defined a diverging beam comparable to that of the triple-scattering experiment, while the polarization was presumably unchanged. The zero for Θ_3 was established by sweeping the telescope through the multiply scattered beam and finding the center of the beam profile, with the energy threshold of the telescope made identical with that used in triple scattering. The asymmetry was then measured.

During the calibration the beam entering the cave was reduced until about 1000 protons/second passed through Counters 1 and 2. The 1-2 coincidences were measured with a fast scaler and used to monitor the beam. The asymmetries $e'_3 = P_1 P_3$ for $\Theta_3 = 13^\circ$ are 0.469 ± 0.011 and 0.432 ± 0.011, for the 12345 and 1234 coincidences respectively.

V. RESULTS

A. Double-Scattering Experiments

In our experimental program we have investigated the polarization produced by the elements reported below (hydrogen and deuterium are to be treated separately). The laboratory-system cross section and polarization results for various nuclei are presented in Table VI, and in graphical form in Figs. 6 to 13. The errors listed are those resulting from counting statistics only. Since the polarization of the incident beam is known to within 4%, there is an additional uncertainty of this amount in the absolute value of the polarization. The energies noted are those obtained from Bragg curves less the amount lost in traversing half of the target. The over-all angular resolution of the measurements may be represented by a gaussian with rms half width of about 1° unless otherwise specified.

Table VI

Cross section and polarization for protons scattered from He, Be, C, Al, Ca, Fe, and Ta with angular resolution as shown in Table II and maximum errors in polarization due to angular misalignment summarized in Table III. The data obtained at small angles with angular resolution as shown in Table IV and maximum errors in the polarization summarized in Table V are denoted by an asterisk. Here Θ is the laboratory-system scattering angle and I_0 is the average laboratory differential cross section in millibarns per steradian for the elastic scattering of protons at the noted mean energy. The absolute cross section is known to 20%, and at larger angles probably contains some inelastic scattering. The errors listed are those due to counting statistics only. The polarization P has, in addition to the counting statistics noted, a 4% absolute uncertainty except for the 289-Mev carbon and 287-Mev aluminum data, in which the absolute uncertainty is 7.5%.

Θ	I_0	P
Helium at 312 Mev		
8	67.5 ± 1.6	0.580 ± 0.028
10	56.1 ± 1.0	0.638 ± 0.019
14	33.3 ± 0.4	0.760 ± 0.011
18	18.0 ± 0.4	0.653 ± 0.023
20	11.7 ± 0.4	0.498 ± 0.043
22	8.30 ±0.18	0.444 ± 0.027
26	3.69 ± 0.15	0.026 ± 0.057
30	1.45 ± 0.10	0.230 ± 0.090
34	0.475 ± 0.08	0.813 ± 0.227

Table VI continued

Θ	I_0	P
Beryllium at 316 Mev		
9	170.0 ± 3.0	0.667 ± 0.022
13	71.0 ± 1.3	0.760 ± 0.011
15	44.2 ± 1.0	0.730 ± 0.015
17	27.2 ± 0.7	0.626 ± 0.026
19	19.1 ± 0.5	0.518 ± 0.027
Carbon at 313 Mev		
2.5*	2602 ± 52	0.036 ± 0.026
3.0*	1376 ± 37	0.104 ± 0.035
3.5*	930 ± 24	0.241 ± 0.034
4.0*	785 ± 23	0.276 ± 0.038
4.13*	758 ± 23	0.282 ± 0.038
4.25*	710 ± 23	0.278 ± 0.040
4.5*	707 ± 24	0.370 ± 0.041
5.0*	647 ± 19	0.401 ± 0.037
6.0*	558 ± 16	0.524 ± 0.033
7.0*	470 ± 15	0.501 ± 0.036
9	270 ± 4.0	0.623 ± 0.014
13	94.5 ± 1.3	0.661 ± 0.017
15	49.9 ± 0.9	0.634 ± 0.020
17	27.4 ± 0.6	0.450 ± 0.026
19	16.9 ± 0.4	0.447 ± 0.028
20	11.6 ± 0.4	0.368 ± 0.034
21	5.86 ± 0.20	0.265 ± 0.042
23	3.75 ± 0.12	0.296 ± 0.042
25	2.31 ± 0.11	0.180 ± 0.063

Table VI continued

Θ	I_0	P
Carbon at 289 Mev		
4.8	495.0 ± 5.0	0.260 ± 0.014
6.8	340.0 ± 3.0	0.498 ± 0.015
7.8	295.0 ± 3.0	0.554 ± 0.016
10	179.0 ± 3.0	0.634 ± 0.024
11.8	117.0 ± 2.0	0.674 ± 0.019
13.8	58.5 ± 0.9	0.659 ± 0.031
15.8	38.8 ± 0.8	0.616 ± 0.034
17.8	18.0 ± 0.6	0.363 ± 0.048
19.8	12.7 ± 0.4	0.410 ± 0.043
21.7	7.12 ± 0.30	0.297 ± 0.064
23.8	5.60 ± 0.24	0.361 ± 0.066
25.8	3.72 ± 0.21	0.112 ± 0.084
27.8	2.95 ± 0.17	0.001 ± 0.085
29.8	2.23 ± 0.18	-0.018 ± 0.125
31.8	1.61 ± 0.15	0.113 ± 0.139
Aluminum at 287 Mev		
7.8	650.0 ± 6.0	0.514 ± 0.011
9.8	323.0 ± 3.0	0.592 ± 0.016
11.8	123.0 ± 2.0	0.611 ± 0.016
13.8	49.4 ± 1.2	0.458 ± 0.033
15.8	17.6 ± 0.7	0.264 ± 0.042
17.8	10.6 ± 0.5	0.319 ± 0.072
19.8	7.29 ± 0.41	0.709 ± 0.078
20.8	7.46 ± 0.34	0.552 ± 0.063
21.8	7.43 ± 0.39	0.570 ± 0.070
23.8	5.09 ± 0.30	0.539 ± 0.085
25.8	2.82 ± 0.23	0.415 ± 0.116

Table VI continued

Θ	I_0	P
Calcium at 310 Mev		
6.8	1200.0 ± 13.0	0.499 ± 0.014
8.8	466.0 ± 8.0	0.584 ± 0.018
10.8	129.0 ± 3.0	0.587 ± 0.029
12.8	30.8 ± 1.5	0.478 ± 0.058
13.3		0.388 ± 0.044
13.8	18.4 ± 0.9	0.437 ± 0.060
14.8	17.1 ± 1.1	0.602 ± 0.079
16.8	17.3 ± 1.3	0.742 ± 0.060
18.8		0.738 ± 0.032
20.8		0.425 ± 0.049
Iron at 315 Mev		
1.5*	502100 ± 8700	0.057 ± 0.025
2.0*	94600 ± 950	-0.056 ± 0.025
2.5*	30260 ± 640	0.025 ± 0.028
3.0*	14820 ± 230	0.146 ± 0.022
3.5*	10000 ± 180	0.185 ± 0.024
4.0*	7320 ± 130	0.269 ± 0.023
5.0*	4550 ± 90	0.348 ± 0.024
6.0*	3000 ± 80	0.384 ± 0.035
3	57270 ± 1580	0.037 ± 0.037
4	9013 ± 110	0.137 ± 0.016
5	4186 ± 37	0.301 ± 0.010
5.8		0.405 ± 0.019
6	2715 ± 26	0.405 ± 0.012
7.8		0.491 ± 0.026
8	976 ± 12	0.508 ± 0.014
9.8		0.517 ± 0.061

Table VI continued

Θ	I_0	P
Iron at 315 Mev (continued)		
10.0	240.0 ± 4.0	0.561 ± 0.014
11.8		0.350 ± 0.070
12	49.6 ± 1.5	0.525 ± 0.034
13	39.1 ± 1.4	0.699 ± 0.038
14	43.4 ± 1.1	0.765 ± 0.024
15.0		0.829 ± 0.086
16	48.3 ± 1.4	0.785 ± 0.027
Tantalum at 316 Mev		
2.5*	241400 ± 6100	-0.011 ± 0.032
3.5*	63700 ± 1700	0.083 ± 0.036
4.5*	26900 ± 900	0.251 ± 0.041
5.5*	10300 ± 500	0.262 ± 0.060
6.5*	3860 ± 450	0.295 ± 0.133
4	41050 ± 450	0.091 ± 0.014
6	6008 ± 75	0.284 ± 0.016
8	823 ± 30	0.418 ± 0.042
10	509 ± 18	0.607 ± 0.037

Helium. There are no excited states of helium, therefore the minimum energy lost in an inelastic collision is the 20 Mev required to remove one nucleon. The detection threshold was placed 15 Mev lower than the mean incident energy, thus the detected protons were elastically scattered. The target contained 1.7 g/cm^2 of liquid helium and was of a type previously used[34] for liquid hydrogen experiments but here modified for additional heat insulation. The geometrical angular resolution for this arrangement varied with scattering angle owing to the nonnegligible dimensions of the helium target. The rms geometrical resolution was 0.8° at $\Theta_2 = 10°$, and increased approximately as sin Θ_2 with increasing Θ_2.

No diffraction effects are apparent in the cross section. However, there is clear evidence (shown in Fig. 6) of a change of sign of polarization at large scattering angles. Theoretical predictions by Tamor,[36] based on the impulse approximation and using questionable nucleon-nucleon phase shifts, do not bear out this feature.

Beryllium. Some data on beryllium are shown in Fig. 7, and over the angular interval studied beryllium behaves in a manner similar to carbon, but with a somewhat higher maximum polarization. The thickness of the target used was 2.1 g/cm^2. The data were taken primarily in order to calibrate the beam that was scattered internally from a beryllium target.

Carbon. Carbon was investigated with both the 315-Mev 76% polarized proton beam (Fig. 8) and the 294-Mev 65% polarized proton beam (Fig. 9). Both sets of data are presented in Table VI. The thickness of the target used for both sets of measurements was 3.2 g/cm^2. Neither of these can be said to display diffraction effects in the cross section nor fluctuations in the polarization. It will be noticed that there is disagreement between the wide-angle elastic scattering cross sections for the two sets of data. This arises from the different energy cutoff used, and indicates again the care with which the wide-angle cross-section data must be interpreted. The curves shown in Fig. 8 are the result of an exact phase-shift calculation by Fermi[37] based on the model he has proposed.[13] The experimental angular resolution has been folded into the theoretical curves for comparison with measurements.

---

[36] S. Tamor, Phys. Rev. 93, 227 (1954); 94, 1087 (1954); 97, 1077 (1955).

[37] E. Fermi (private communication)

Aluminum. Aluminum is the lightest element we have investigated in which the diffraction pattern and fluctuations in polarization are clearly discernible (Fig. 10). The thickness of the target used was 5 g/cm^2. The polarization minimum occurs at a slightly smaller angle than the cross-section diffraction minimum, and the second polarization maximum is closely associated with the secondary diffraction maximum.

Theoretical curves of the average differential cross section and polarization for a parabolic central potential--with phase shifts calculated in the WKB approximation by Fernbach, Heckrotte, and Lepore[22]--are shown along with the experimental data for 285-Mev protons on aluminum. The potential used was

$$V = -(u + iw)(1 - r^2/R^2) - \frac{2\mu a^2}{\hbar R^2}\, \underset{\sim}{g} \cdot \underset{\sim}{L} \qquad (r < R), \qquad (22)$$

$$V = 0, \qquad (r > R),$$

with u = 18 Mev, w = 30 Mev, $\mu a^2 = 4.77 \times 10^{-26}$ Mev/cm^2, and $R = 1.6\, A^{1/3} \times 10^{-13}$ cm. The additional scattering due to the Coulomb potential of the nucleus was included in this calculation. A similar calculation for neutrons is also shown in Fig. 10, and it is apparent from the two curves that Coulomb nuclear interference effects can cause large alterations in the polarization at angles at which the Coulomb cross section itself is quite negligible.

On the graphs in Fig. 10 a third curve shows the result of folding a gaussian angular resolution curve of $\sigma = 1.1^\circ$ into the calculation for protons, using the potential given by Eq. (22). The experimental minima in both cross section and polarization are less pronounced than the theoretical predictions. To some extent the discrepancy may be due to the acceptance of inelastically scattered protons. Experimentally the minima occur at slightly larger angles than predicted, which may be the result of using the WKB approximation for the phase shifts. Extensive calculations for cross section and polarization of protons and neutrons from aluminum, using a Woods and Saxon type potential, have been carried out by Sternheimer.[20] Also included are calculations for the rotation parameter R and the rotation angle β. The agreement with the

used to calculate the nuclear scattering was

$$V = -(u + iw)(1 - r^2/R^2) \mp \frac{2\mu a^2}{hR^2}(1 - i)\,\sigma \cdot L, \quad (r \leq R), \tag{23}$$

$$V = 0, \quad (r > R),$$

where the values of the parameters are the same as specified in Eq. (22). The sign of the spin-orbit potential that corresponds to the choice of the shell model is represented in Eq. (23) by the negative sign and leads to curve (a) in Fig. 14, whereas curve (b) was obtained with the opposite choice of sign. Relativistic corrections to the Coulomb potential were included to order v/c.

Iron. Measurements of the iron differential cross section and polarization are shown in Fig. 15. The square points were obtained with an rms angular resolution of 0.42° while the circle points represent the small-angle portion of the data previously displayed in Fig. 12 with 1.0° rms angular resolution. Curves have been drawn through the experimental points for each set of data in order to distinguish the measurements obtained with different angular resolutions. Several statements can be made concerning the divergence of the two curves. At the largest angles measured the slopes of the cross sections for the two curves are similar. Since these were independent measurements the small difference in magnitude (~10%) represents an approximate lower limit on the absolute error in the cross sections reported. In order to more correctly compare these cross sections (which were obtained with different angular resolutions) a gaussian resolution function with $\sigma = 0.91^\circ$ was folded into the curve representing the 0.42° resolution data and the resulting curve was compared to the 1.0° angular resolution data. This led to a more realistic estimate of 20% as the absolute accuracy of the cross-section measurements. The relative angular dependence of the differential cross section is presumably unaffected by systematic errors of the type. Next it should be noted that the cross-section curve with 1.0° angular resolution shows the rise due to Coulomb scattering at a larger angle than the corresponding curve with 0.46° resolution. This discrepancy is of course due to the rapidly increasing Coulomb cross section as observed in the two experiments by counters with different angular resolutions. The fold of a gaussian with $\sigma = 0.91^\circ$ into the 0.46°-resolution

experiments is very good in some respects; however, there is no single potential that fits all the experiments.

Calcium, Iron, and Tantalum. Calcium (Fig. 11) and iron (Fig. 12) display cross-section and polarization curves similar to aluminum, and the above discussion applies also to them. The first polarization maximum is seen to be increasingly suppressed as the atomic number becomes larger, in keeping with the observations on Coulomb effects in aluminum. The measurements on tantalum (Fig. 13) show the complete disappearance of the first polarization maximum.

The triangular points on the polarization graphs of calcium and iron represent data taken with a slightly different energy cutoff. The polarization is sufficiently insensitive to small threshold changes that it was felt permissible to include the measurements on the same graph. The cross section, however, depends critically on the energy cutoff, and therefore the corresponding cross-section measurements have not been included. The square points on the tantalum graph were obtained in the small-angle measurements with an rms angular resolution of 0.46°. The target thicknesses used for the measurements on calcium, iron, and tantalum were 3.8 g/cm^2, 2.6 g/cm^2, and 1.3 g/cm^2, respectively.

B. Small-Angle Measurements

Carbon. The small-angle carbon differential cross section and polarization, shown in Fig. 14, were obtained with an rms angular resolution of 0.35°. The thickness of the target used was 1.0 g/cm^2. No interference effects between the Coulomb and nuclear scattering were discernible in the angular dependence of the differential cross section. The two curves shown with the polarization data have been calculated by Warren Heckrotte,[38] using a complex gradient type spin-orbit potential as well as the usual complex central potential. Such a model implies the existence of a spin-dependent force for protons inelastically scattered from nuclei. The specific potential

[38] W. Heckrotte, Phys. Rev. (in press).

cross-section data resulted in a curve whose angular dependence and magnitude were similar to those of the curve representing the 1.0°-resolution data. Similar conclusions can be drawn regarding the polarization curves shown also in Fig. 15. The folding procedure was carried out by using the 0.42° angular resolution cross-section data at $\Phi = 0^{\circ}$ and at $\Phi = 180^{\circ}$. The polarization was calculated from the resulting cross-section curves and was found to be in good agreement with the measurements of the polarization with 1.0° resolution. In summary it is believed that both sets of data are in agreement, with regard to the angular dependence of the cross section and polarization; however, in comparisons with theoretical predictions the 0.42° angular resolution data should be used.

The polarizations measured at $\Theta = 1.5^{\circ}$, 2.0°, and 2.5° have large systematic errors ($\Delta P \approx 0.09$) hence no significance should be attached to the oscillation in sign of the polarization in this region. The systematic polarization errors at the larger angles (3° to 6°) are much smaller, i.e, $\Delta P < 0.02$, and can be neglected in comparison with the errors due to counting statistics.

Tantalum. The tantalum measurements with 0.46° angular resolution are shown in Fig. 13 along with the data obtained with 1.0° resolution. The thickness of the target used was 0.27 g/cm^2. The angular range of the measurements includes mainly the nuclear scattering. The rise due to Coulomb scattering was observed only at the smallest angle measured (2.5°). No attempt was made to observe smaller scattering angles because of the large systematic errors, which would have been present because of small angular misalignments (i.e., $\Delta P > 0.10$ for $\Delta\Theta = 0.02$).

C. Triple-Scattering Experiments

The values obtained for R as a function of Θ for aluminum are shown in Fig. 16. Also shown are the two possible values of β for each R.

It might be expected from a comparison of Eqs.(5) and (28) that in an angular region where the polarization displays a dip, β should also undergo significant variation. Figure 16 shows, however, that this is not the case. The angular resolution in this experiment was nearly twice as large as in double scattering, yet was not so poor as to obscure any variations over as wide an angular interval as the dip in P.

A curve of R calculated by Dr. Heckrotte with the same well parameters as used for calculating I_0 and P for aluminum is included in Fig. 16.

Several early experiments on triple scattering were done to investigate R for carbon. The techniques differed only slightly from those described above. The results, along with other triple-scattering data, are tabulated in Table VII.

D for Aluminum and Carbon. In agreement with the requirements for a spin-zero nucleus, D for carbon is seen from Table VII to be, within statistics, equal to 1. The techniques used to investigate D for aluminum therefore appear to be sound.

Aluminum 12° left and 12° right give values for D that are not statistically different from 1; thus the result is not in disagreement with the assumption made, in calculating the polarization from various elements, that for elastic scattering all complex nuclei behave as if they had zero spin.

VI. MECHANISM OF POLARIZATION; DISCUSSION OF RESULTS

The scattering of protons on nuclei can be considered according to different models that are valid under different circumstances. At our high energy we may think of two limiting cases: (a) elastic scattering on the nucleus as a whole, and (b) elastic scattering on a nucleon of the nucleus. The intermediate cases, in which one takes into account the complex excitation phenomena of the target, are too complicated to be interpreted at present.

In Case (a) the nucleus can be described by a central potential well $V_c(r)$, which is chosen to be complex in order to account for the absorption of nucleons in nuclear matter, thus

$$V_c = V_1(r) + i\, V_2(r). \tag{24}$$

To this central potential a spin-dependent term $V_s(r)$ is added, where

$$V_s = -\mu \frac{1}{r} \frac{dV_1}{dr} \underline{\sigma} \cdot \underline{L} \tag{25}$$

Table VII

Rotation and depolarization for protons scattered from aluminum and carbon

R FOR ALUMINUM AND CARBON

$$R = -e_{3s}/e'_3 = \sqrt{1 - P_2^2}\cos(\theta-\beta) \quad (\Phi_2 = 270^\circ)$$

Θ_2	Θ_3	$-e_{3s}$	e'_3	R	P_2	β	β
Aluminum at 300 Mev							
9.9°	12.95°	0.297 ± .022	0.469 ± .011	0.633 ± .049	0.59 ± .05	$-29^\circ \pm 6^\circ$	$48^\circ \pm 6^\circ$
13.8°	13.00°	0.270 ± .032	" ± "	0.576 ± .069	0.46 ± .05	$-36^\circ \pm 6^\circ$	$63^\circ \pm 6^\circ$
17.0°	13.05°	0.226 ± .047	" ± "	0.482 ± .100	0.27 ± .06	$-43^\circ \pm 7^\circ$	$77^\circ \pm 7^\circ$
21.7°	13.10°	0.198 ± .040	" ± "	0.422 ± .085	0.57 ± .08	$-37^\circ \pm 8^\circ$	$81^\circ \pm 8^\circ$
Carbon at 290 Mev							
10.4°	13.5°	0.362 ± .050	0.428 ± .029	0.846 ± .129	0.65 ± .04		
10.4°	12.0°	0.287 ± .075	0.533 ± .051	0.538 ± .156	0.65 ± .04		
10.4°	Average			0.717 ± .100		$-9^\circ \pm 18^\circ$	$30^\circ \pm 18^\circ$
14.1°	12.0°	0.180 ± .080	0.533 ± .051	0.338 ± .154	0.65 ± .04	$-50^\circ \pm 13^\circ$	$78^\circ \pm 13^\circ$

D FOR ALUMINUM AND CARBON

$$D = \frac{1}{\cos\Phi_2}\left[\frac{e_{3n}}{e'_3}(1 + P_1P_2\cos\Phi_2) - \frac{P_2}{P_1}\right]$$

Θ_2	Φ_2	Θ_3	e_{3n}	e'_3	P_1P_2	P_1	D
Aluminum at 310 Mev							
12°	0°	14.7°	0.695 ± .037	0.469 ± 0.030	0.421 ± .034	0.69 ± .05	1.22 ± .20
12°	180°	14.5°	-0.139 ± .066	0.469 ± 0.030	0.421 ± .034	0.69 ± .05	1.06 ± .11
Carbon at 310 Mev							
12°	180°	14.3°	-0.074 ± .055	0.469 ± 0.030	0.469 ± .037	0.69 ± .05	1.07 ± .08

Such a spin-orbit potential is similar to the one proposed by M. G. Mayer[39] and by Haxel Jensen, and Suess[40] to account for nuclear shell structure, and bears a formal resemblance to the Thomas precession term.

It has been shown by many authors[13, 26,] that potentials of the form $V(r) = V_c(r) + V_s(r)$ give rise to polarization in the elastic scattering process. Following the treatment by Fermi,[13] who has calculated the scattering from such a potential specialized to a square well of radius R with real and imaginary well depths -B and $-B_A$ respectively, the scattered amplitude $f(\theta, \phi) = g(\theta) + h(\theta)\sigma \cdot n$ is given in Born approximation as

$$g(\theta) = -\frac{2M}{\hbar^2}(B + iB_A) R^3 \left(\frac{\sin q}{q^3} - \frac{\cos q}{q^2}\right),$$

$$h(\theta) = -\frac{2M}{\hbar^2} i\mu\hbar BR^3k^2 \sin\theta \left(\frac{\sin q}{q^3} - \frac{\cos q}{q^2}\right), \tag{26}$$

where $q = 2kR \sin\theta/2$, M is the proton mass, and $p = k\hbar$ is the momentum of the incident proton. The magnitude of the spin-orbit coupling μ was inferred from the spin-orbit splitting of the nuclear levels as $\mu = 15 \frac{\hbar}{2M^2c^2}$. From Eqs. (6) and (3) the average differential cross section and polarization are

$$I_0 = |g|^2 + |h|^2 = \frac{4M^2}{h^2} R^6B^2 \left\{\frac{\sin q}{q^3} - \frac{\cos q}{q^2}\right\}^2 \left\{1 + \left(\frac{B_A}{B}\right)^2 + \frac{225}{4}\left(\frac{p}{Mc}\right)^2 \sin^2\theta\right\},$$

$$P = \frac{2 \operatorname{Re} g^*h}{|g|^2 + |h|^2} = \frac{15\left(\frac{p}{Mc}\right)^2 \frac{B_A}{B} \sin\theta}{1 + \left(\frac{B_A}{B}\right)^2 + \frac{225}{4}\left(\frac{p}{Mc}\right)^2 \sin^2\theta}. \tag{27}$$

Equations (26) and (27) illustrate several of the characteristic features of the polarization by scattering, notably that the polarization vanishes if either B or B_A is zero. A particular feature of the Born-approximation calculation is the prediction that the polarization is independent of the nuclear radius and

[39] M. G. Mayer, Phys. Rev. 78, 16 (1950).
[40] Haxel, Jensen, and Suess, Ann. Physik 128, 295 (1950).

shape of the nuclear potential, but depends only upon the relative magnitudes of B, B_A, and μ. To the extent that these parameters are the same for all nuclei one would expect the magnitude and angular distribution of the polarization to be the same for all elements. Using as the magnitude of the parameters B = 18 Mev, B_A = 16 Mev, and μ as required by the shell model, one obtains reasonable agreement for the observed polarization from carbon for $\theta < 18^\circ$. More exact calculations[22] indicate that, to within the accuracy to which the other constants are known, changes of a factor of two in μ would not be in disagreement with the experimental results for polarization. In the Born approximation the real and imaginary parts of the central potential V_c contribute to the real and imaginary parts respectively of g, while the real spin-orbit potential produces an imaginary h. This is approximately true in the exact calculation, thus from Eq. (5) it is seen that a real central potential suppresses the maximum polarization, thus preventing the realization of 100% polarized beams.

It has been shown by several authors[22, 36, 41] that the existence of the spin-orbit term in the equivalent nuclear potential describing the nucleon-nucleus interaction follows as a consequence of the spin dependence of the nucleon-nucleon interaction. Detailed phase-shift calculations, using various well shapes, well depths, and strengths for the spin-orbit coupling, have been carried out, notably by Sternheimer[20] and by Fernbach, Heckrotte, and Lepore.[22]

From Eq. (27) it is seen that the sign of the spin-orbit potential determines the sign of the polarization. A phase-shift expansion for $g(\theta)$ substantiates the Born-approximation conclusion that a change in sign of the spin-orbit potential will reverse the sign of the polarization. The exact expressions show that interchanging phase shifts for $j = l + 1/2$ changes the sign of $h(\theta)$, but leaves $g(\theta)$ nearly unaltered. From Eq. (3) it is evident that this results in a change in sign of P. Marshall and Marshall[31] and (independently) Brinkworth and Rose[32] have measured the sign of the polarization by degrading high-energy polarized proton beams to 10 Mev and observing the asymmetry produced in the well-known resonance scattering from helium. Their results

---

[41] G. Takeda and K. M. Watson, Phys. Rev. 97, 1336 (1955).

both call for the same sign of spin-orbit potential as used in the shell model. The small-angle polarization measurements from carbon reported in this paper have been analyzed by W. Heckrotte,[38] using a complex spin-orbit coupling (see Eq. (23) and discussion of small-angle carbon measurements). His conclusion regarding the sign of the polarization is in agreement with the above-mentioned authors.

The rotation parameter R that is measured in the triple-scattering experiments is related to the rotation angle β through Eq. (16). It has been shown by Wolfenstein[21] that

$$\sin \beta = - \frac{2 \, \mathrm{Im} \; g^* h}{I_0 \sqrt{1 - P^2}} \quad . \tag{28}$$

In the Born approximation g and h are given by Eqs. (26) thus:

$$\sin \beta = - \frac{B}{B_A} \frac{P}{\sqrt{1 - P^2}} \tag{29}$$

From Eq. (29) it follows that a knowledge of the sign of β will determine the sign of the polarization P. Equation (16) shows that triple-scattering measurements determine only $\cos (\Theta - \beta)$ and thereby admit of two values of β which are opposite in sign and for small Θ approximately equal in magnitude. There is sufficient latitude in nuclear well parameters to fit both of the possible magnitudes of β with either sign of the spin-orbit coupling, thus in view of the accuracy to which the parameters of such a theory are known we conclude that the triple-scattering measurements do not give certain information on the sign of the spin-orbit coupling.

In the Born approximation a characteristic feature (which is independent of the well shape chosen) is that $g(\theta)$ and $h(\theta)/\sin \theta$ have the same angular dependence. This gives rise to the smoothly varying polarization angular distribution shown by Eq. (27). Exact phase-shift calculations show that these functions pass through the diffraction zero at slightly different angles. This results in a polarization angular distribution that exhibits an oscillation in the region of the diffraction minimum. Such effects have been observed in the data reported in this paper.

VII. ACKNOWLEDGMENTS

Much assistance during the many days of cyclotron time necessitated by the experiments has been generously supplied by Dr. Gordon Pettengill and by various graduate students, especially Messrs. John Baldwin, David L. Fischer, and Richard C. Weingart. Discussions of polarization theory with Dr. Lincoln Wolfenstein have been invaluable. The theoretical help of Drs. Burton Fried, Joseph V. Lepore, Warren Heckrotte, and Henry P. Stapp is gratefully acknowledged.

The authors wish to thank Mr. James Vale and the cyclotron crew for providing the polarized proton beam, and the accelerator technicians for constructing much of the equipment.

This work was done under the auspices of the United States Atomic Energy Commission.

LEGENDS

Fig. 1. Plan view of the cyclotron and orbit of the polarized beam. If the cyclotron is viewed from above the spin of the polarized beam is upward.

Fig. 2. Schematic diagram of the scattering planes in the measurement of the rotation parameter R.

Fig. 3. Scale drawing of the three counter telescope used for the double scattering measurements.

Fig. 4. Integral range curves for protons scattered from carbon.

Fig. 5. Azimuthal dependance of the carbon differential cross section at $\Theta_2 = 12^\circ$.

Fig. 6. Helium average differential cross section and polarization at 312 Mev.

Fig. 7. Beryllium average differential cross section and polarization at 316 Mev.

Fig. 8. Carbon average differential cross section and polarization at 313 Mev. The curves shown are the result of an exact phase shift calculation for the model proposed by Fermi[13, 33] with the experimental angular resolution folded in.

Fig. 9. Carbon average differential cross section and polarization at 289 Mev.

Fig. 10. Aluminum average differential cross section and polarization at 287 Mev. The graphs shown represent the theoretical curves of Fernbach, Heckrotte and Lepore[22] for the scattering of neutrons and protons from aluminum and a graph for protons with the experimental angular resolution folded in.

Fig. 11. Calcium average differential cross section and polarization at 310 Mev.

Fig. 12. Iron average differential cross section and polarization at 315 Mev.

Fig. 13. Tantalum small angle average differential cross section and polarization at 315 Mev. The square points were obtained with an rms angular resolution of 0.46° whereas the circle points were obtained with 1.0° rms angular resolution.

Fig. 14. Carbon small angle differential cross section and polarization at 313 Mev. The curves shown with the polarization data were obtained by Heckrotte[34] using a complex gradent type spin-orbit potential and relativistic Coulomb potential to order v/c. Curve (a) represents the choice of sign of the nuclear spin-orbit potential the same as the shell model assignment. Curve (b) corresponds to the opposite choice of sign.

Fig. 15. Iron small angle average differential cross section and polarization at 315 Mev. The square points were obtained with an rms angular resolution of 0.42^{o} whereas the circle points were obtained with 1.0^{o} rms angular resolution.

Fig. 16. Upper graph: Rotation function R vs laboratory scattering angle Θ for aluminum at an average energy of 300 Mev. The curve shown has been calculated by Heckrotte using the same potential as in Fig. 10.

Lower graph: Two possible angles of rotation β vs Θ for aluminum at 300 Mev.

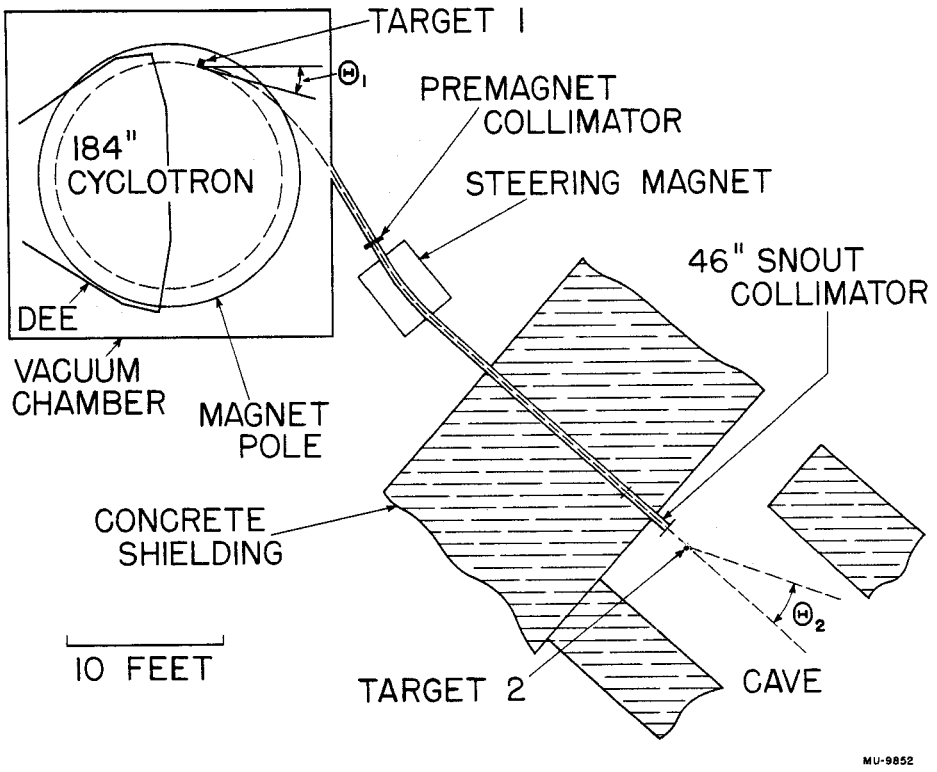

Fig. 1. Plan view of the cyclotron and orbit of the polarized beam. If the cyclotron is viewed from above the spins of the polarized beam is upward.

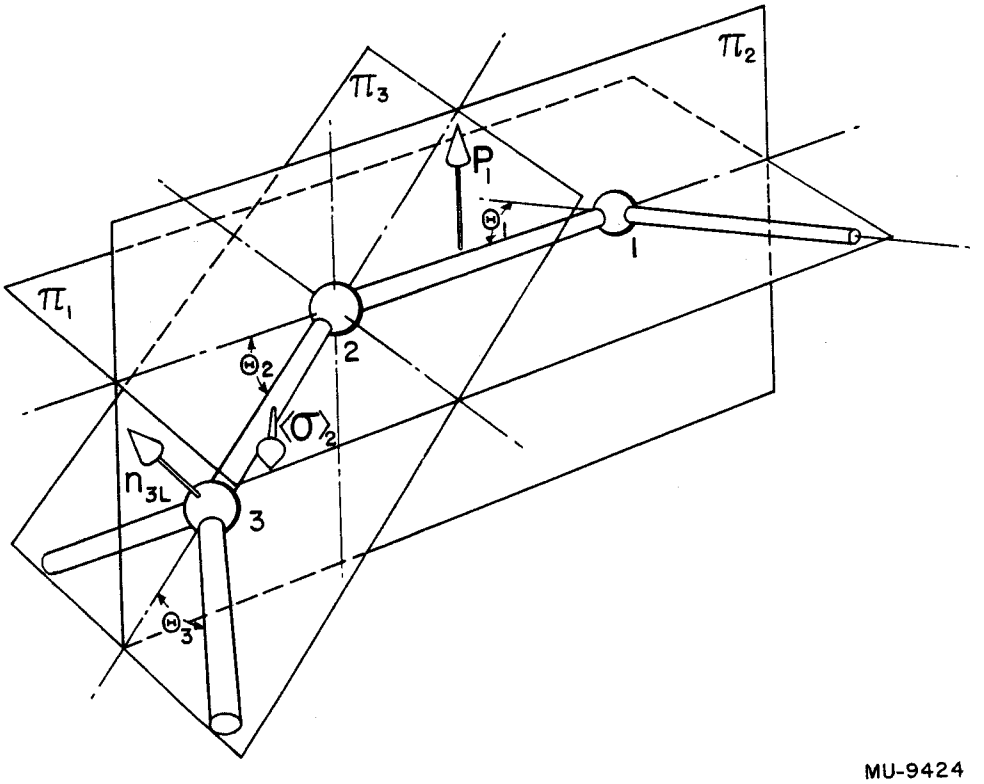

Fig. 2. Schematic diagram of the scattering planes in the measurement of the rotation parameter R.

Fig. 15. Iron small angle average differential cross section and polarization at 315 Mev. The square points were obtained with an rms angular resolution of 0.42° whereas the circle points were obtained with 1.0° rms angular resolution.

Fig. 16. Upper graph: Rotation function R vs laboratory scattering angle Θ for aluminum at an average energy of 300 Mev. The curve shown has been calculated by Heckrotte using the same potential as in Fig. 10.

Lower graph: Two possible angles of rotation β vs Θ for aluminum at 300 Mev.

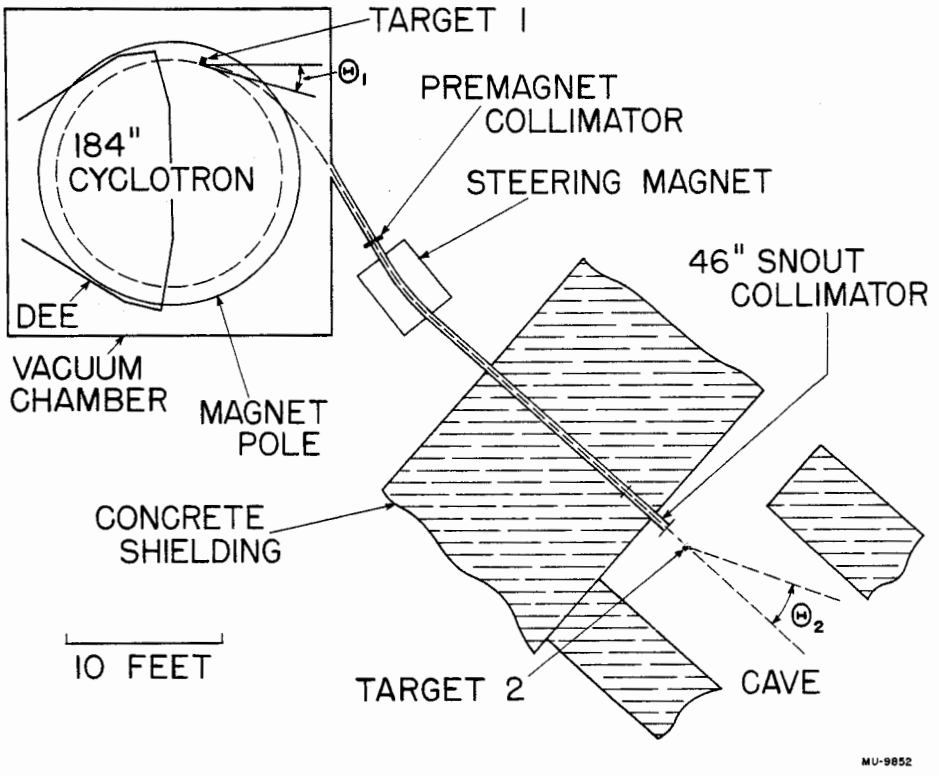

Fig. 1. Plan view of the cyclotron and orbit of the polarized beam. If the cyclotron is viewed from above the spins of the polarized beam is upward.

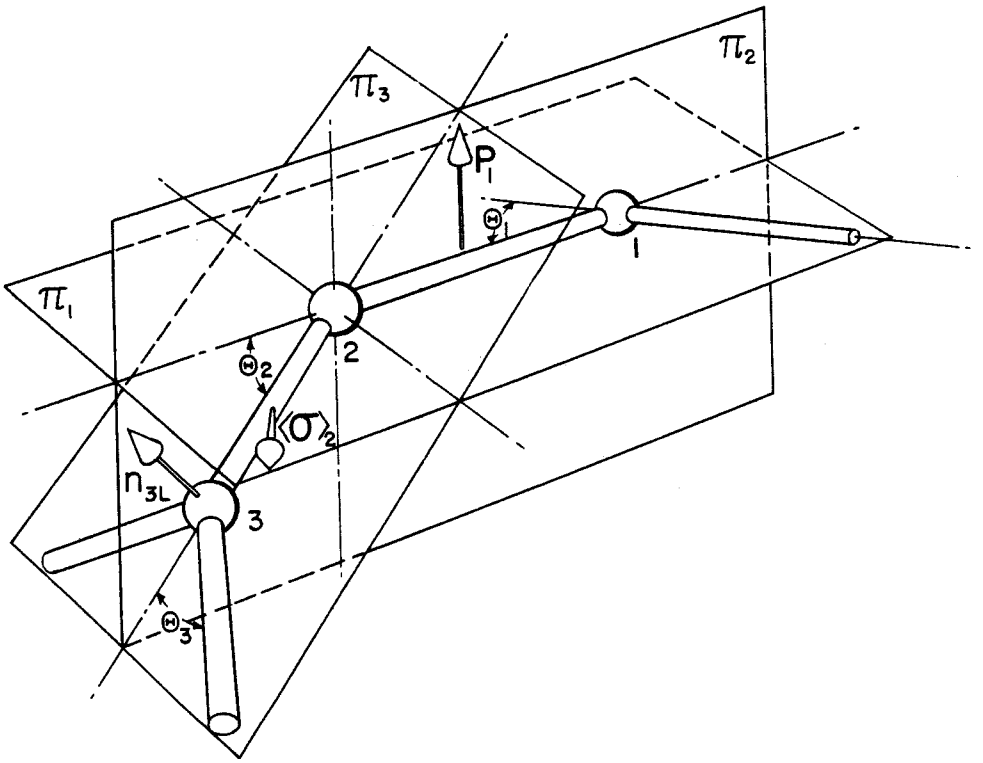

Fig. 2. Schematic diagram of the scattering planes in the measurement of the rotation parameter R.

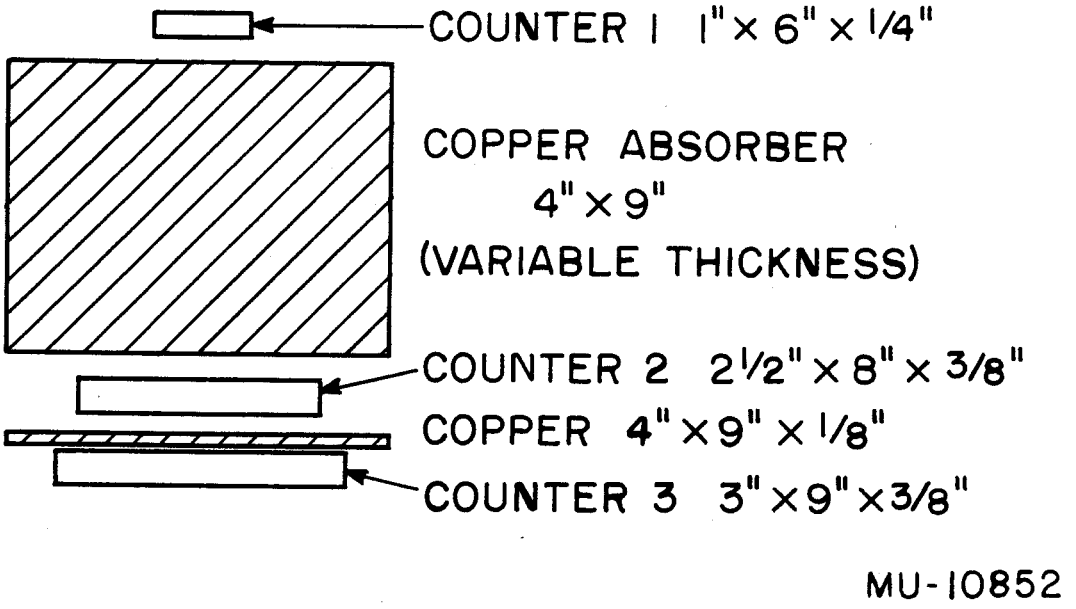

Fig. 3. Scale drawing of the three counter telescope used for the double scattering measurements.

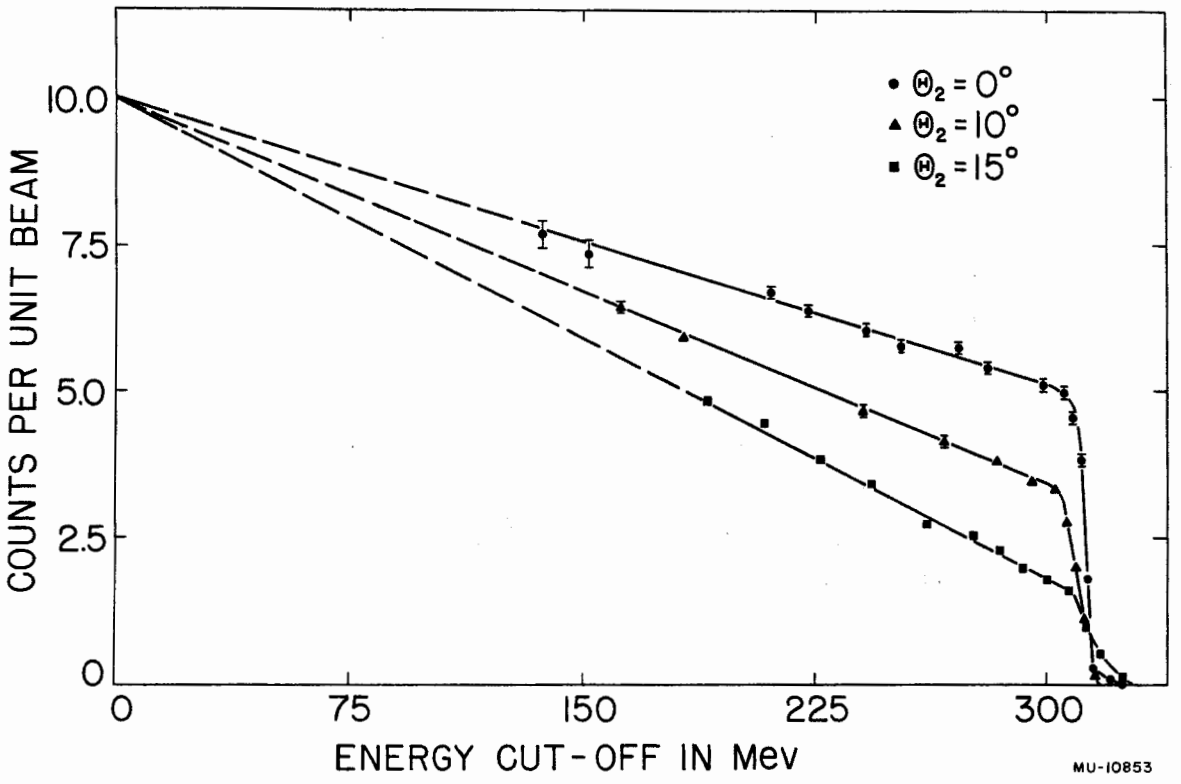
• $\Theta_2 = 0°$
▲ $\Theta_2 = 10°$
■ $\Theta_2 = 15°$
COUNTS PER UNIT BEAM
10.0
7.5
5.0
2.5
0
0
75
150
225
300
ENERGY CUT-OFF IN Mev
MU-10853

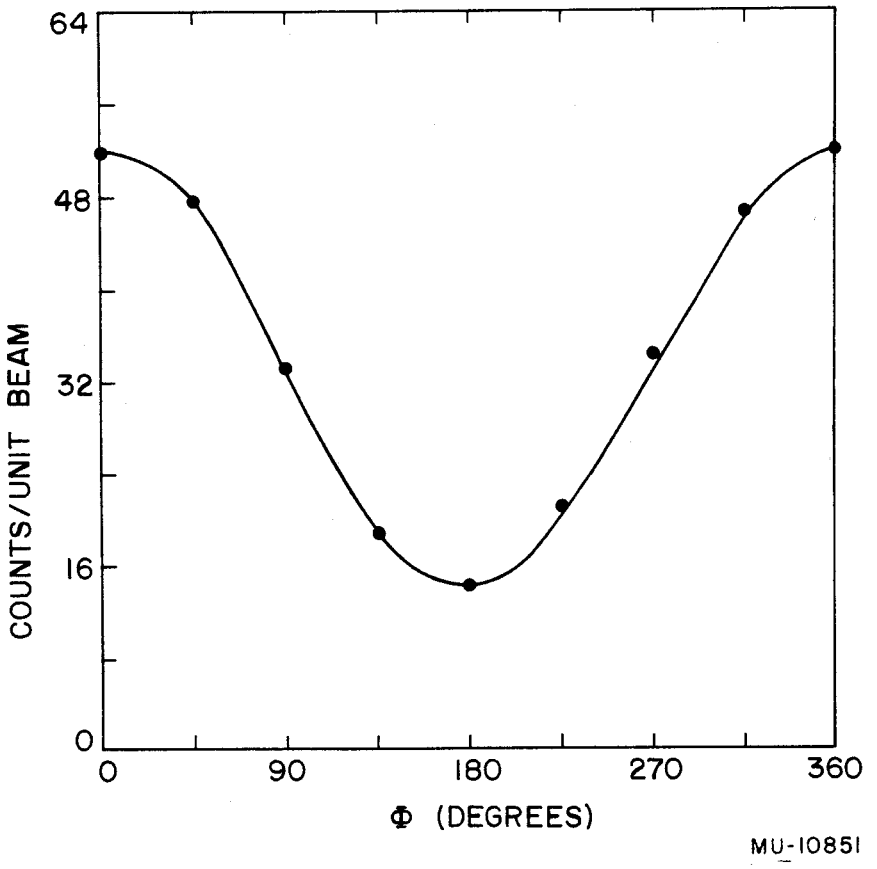

Fig. 5. Azimuthal dependance of the carbon differential cross section at $\Theta_2 = 12^{\circ}$.

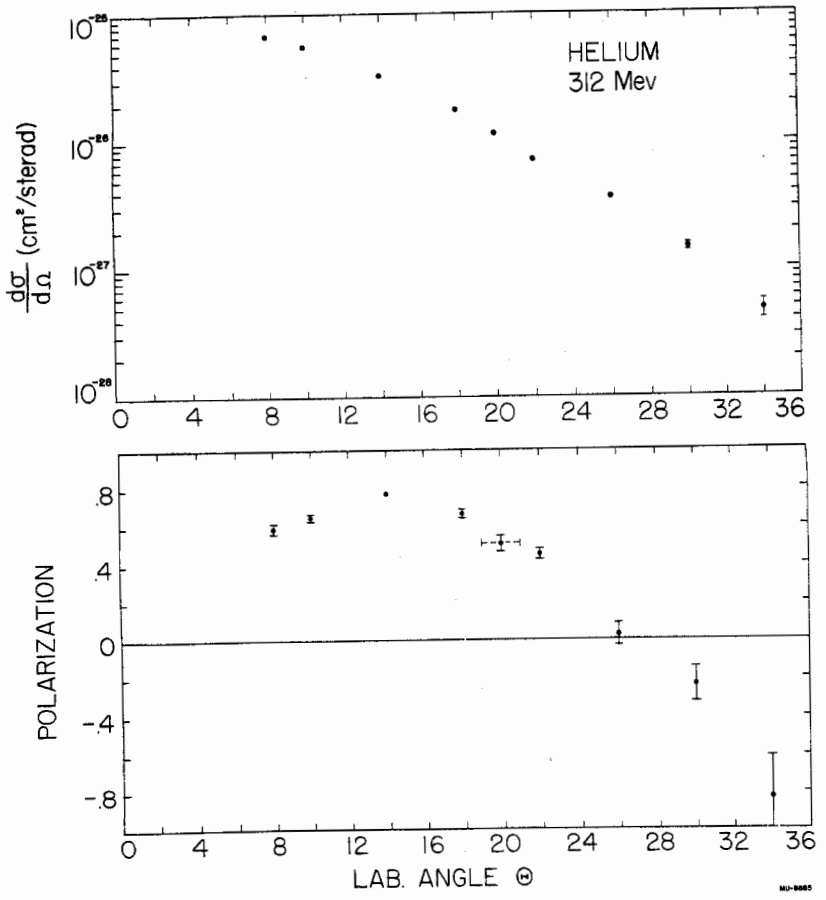

Fig. 6. Helium average differential cross section and polarization at 312 Mev.

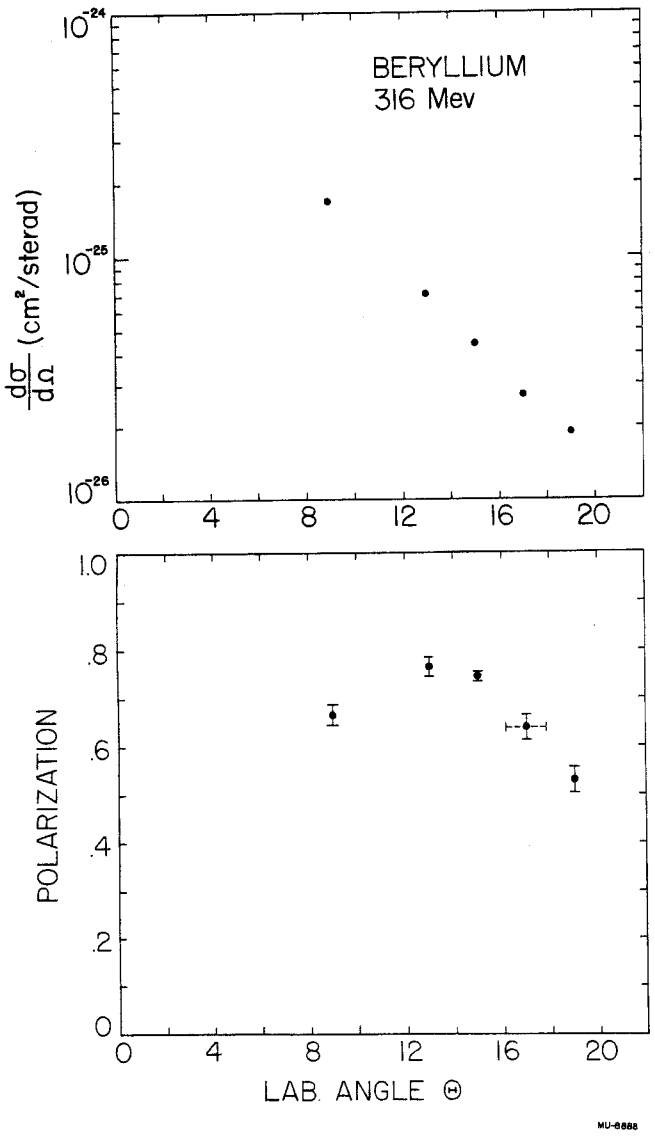

Fig. 7. Beryllium average differential cross section and polarization at 316 Mev.

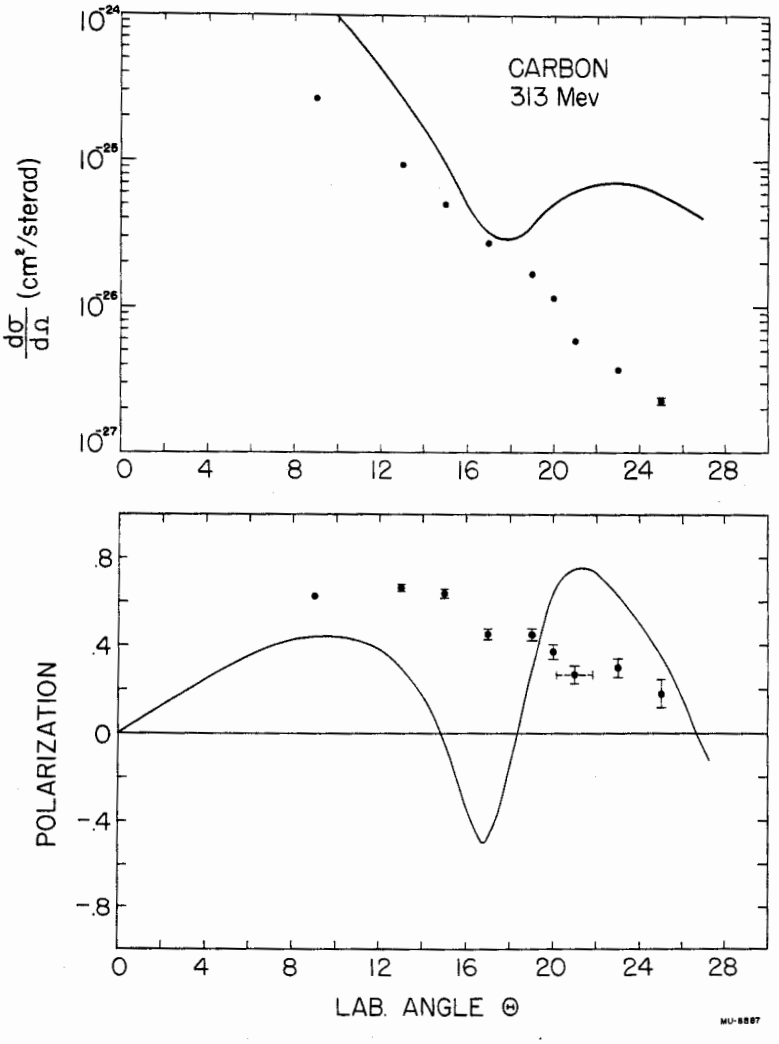

Fig. 8. Carbon average differential cross section and polarization at 313 Mev. The curves shown are the result of an exact phase shift calculation for the model proposed by Fermi [13, 33] with the experimental angular resolution folded in.

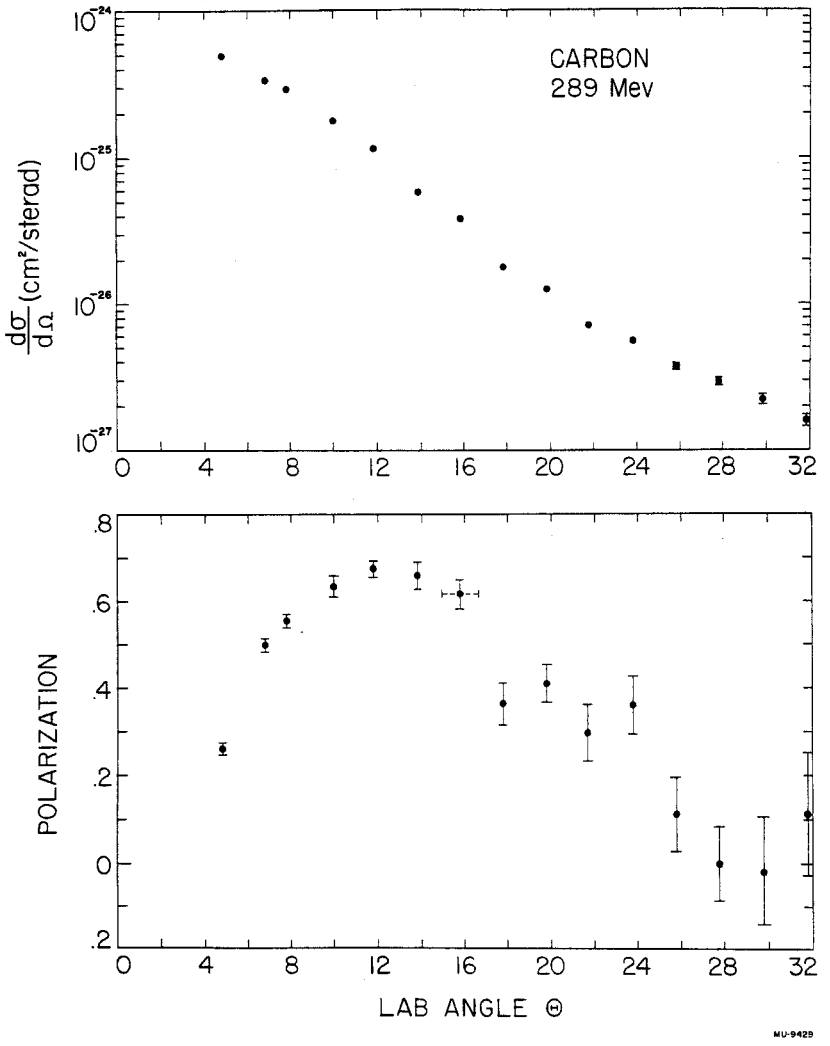

Fig. 9. Carbon average differential cross section and polarization at 289 Mev.

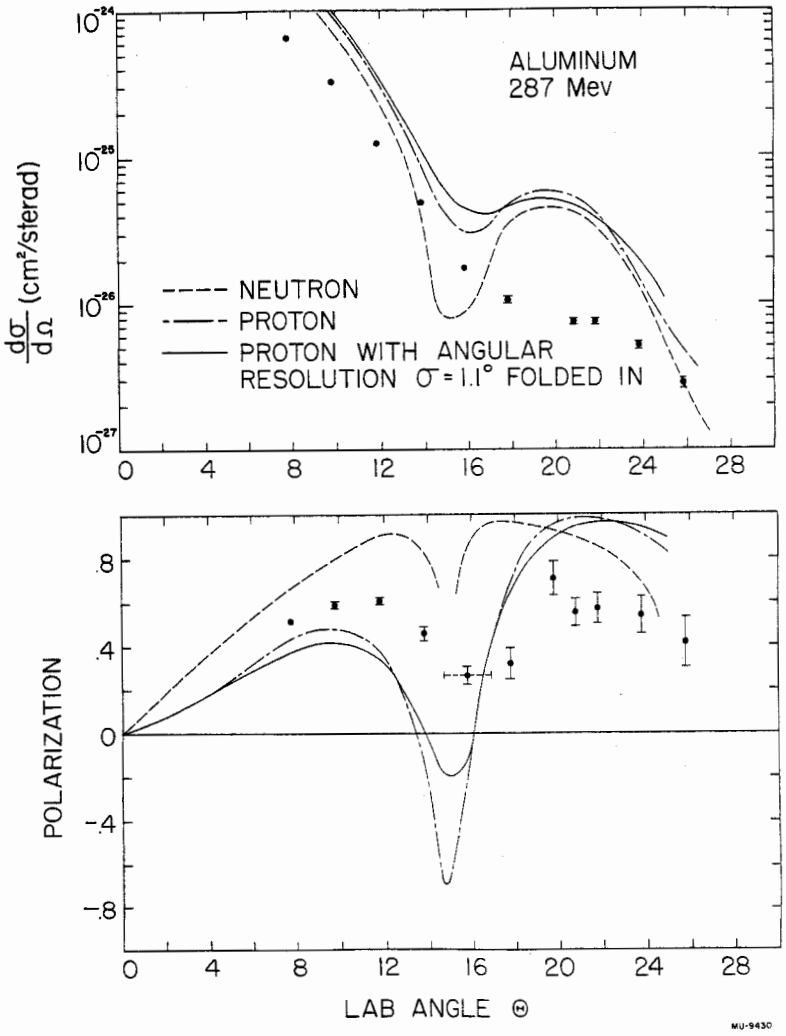

Fig. 10. Aluminum average differential cross section and polarization at 287 Mev. The graphs shown represent the theoretical curves of Fernbach, Heckrotte and Lepore[22] for the scattering of neutrons and protons from aluminum and a graph for protons with the experimental angular resolution folded in.

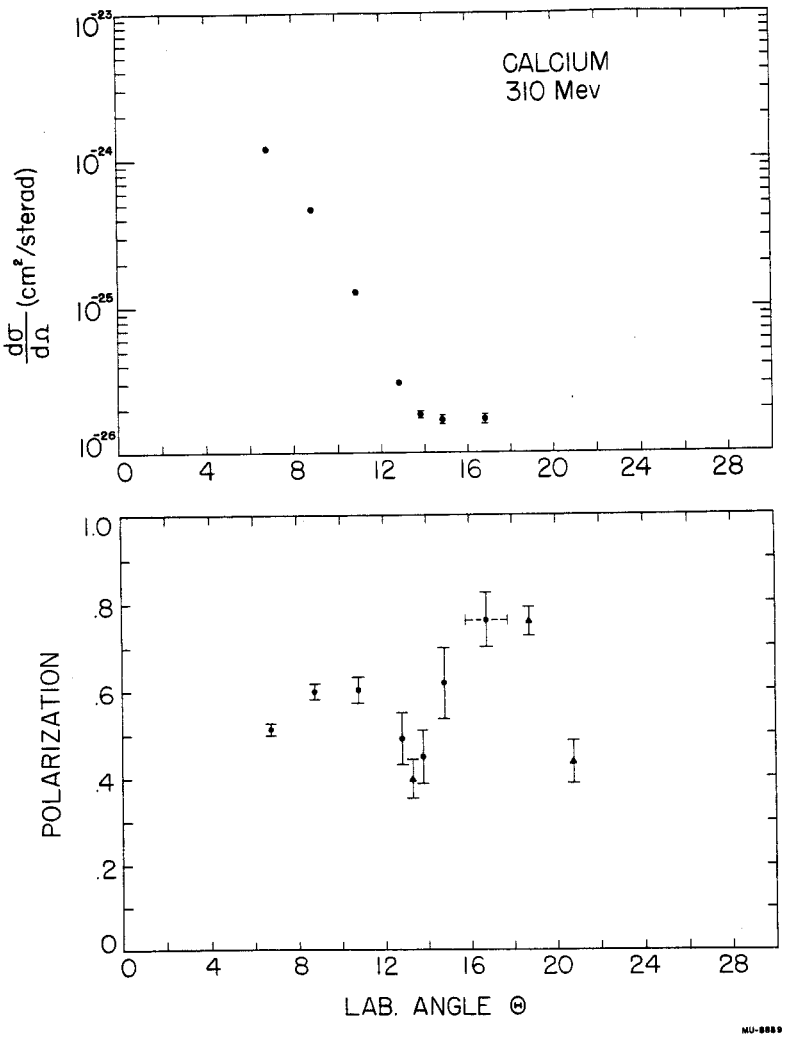

Fig. 11. Calcium average differential cross section and polarization at 310 Mev.

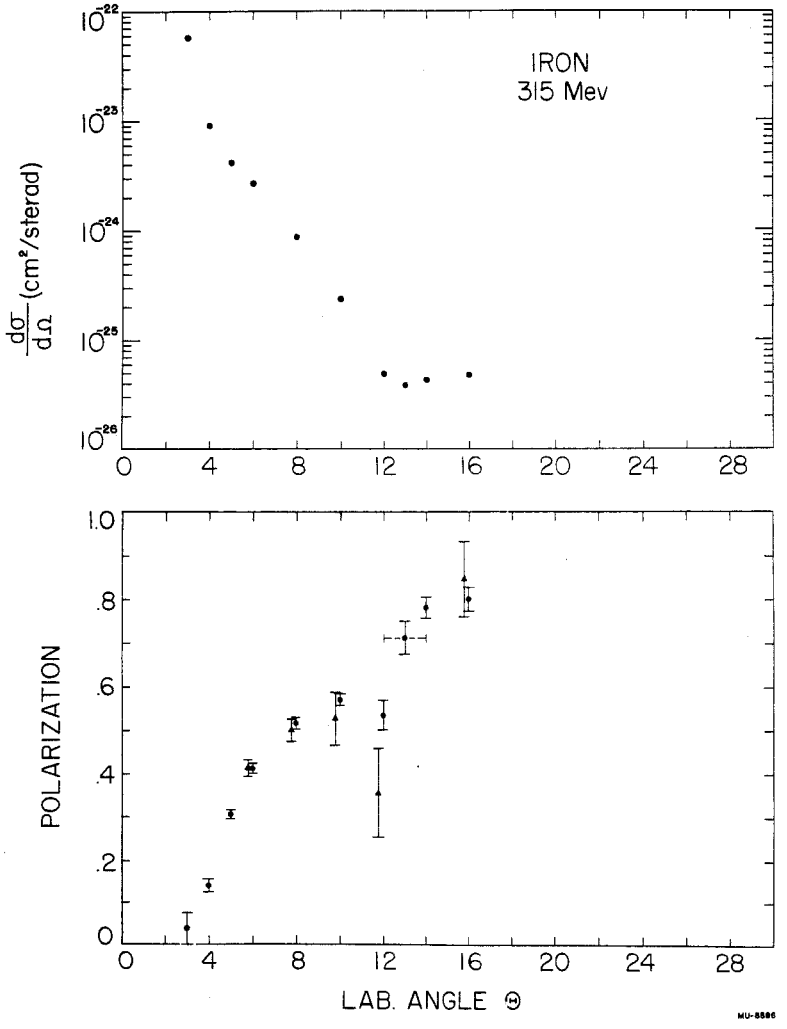

Fig. 12. Iron average differential cross section and polarization at 315 Mev.

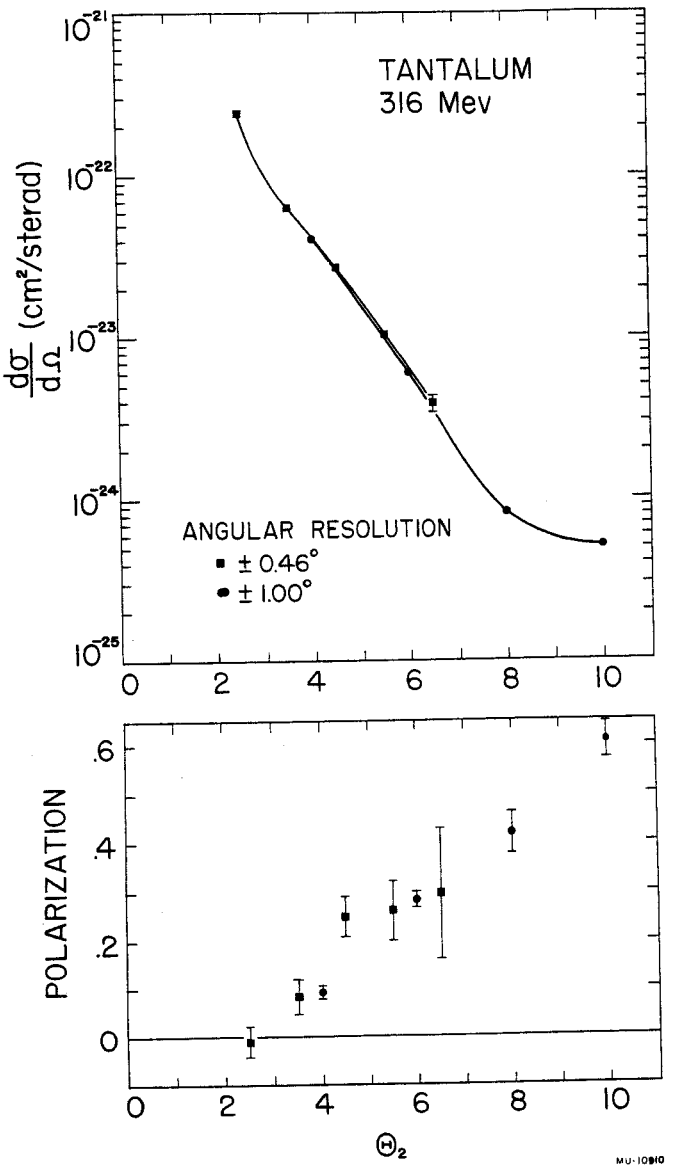

Fig. 13. Tantalum small angle average differential cross section and polarization at 315 Mev. The square points were obtained with an rms angular resolution of 0.46° whereas the circle points were obtained with 1.0° rms angular resolution.

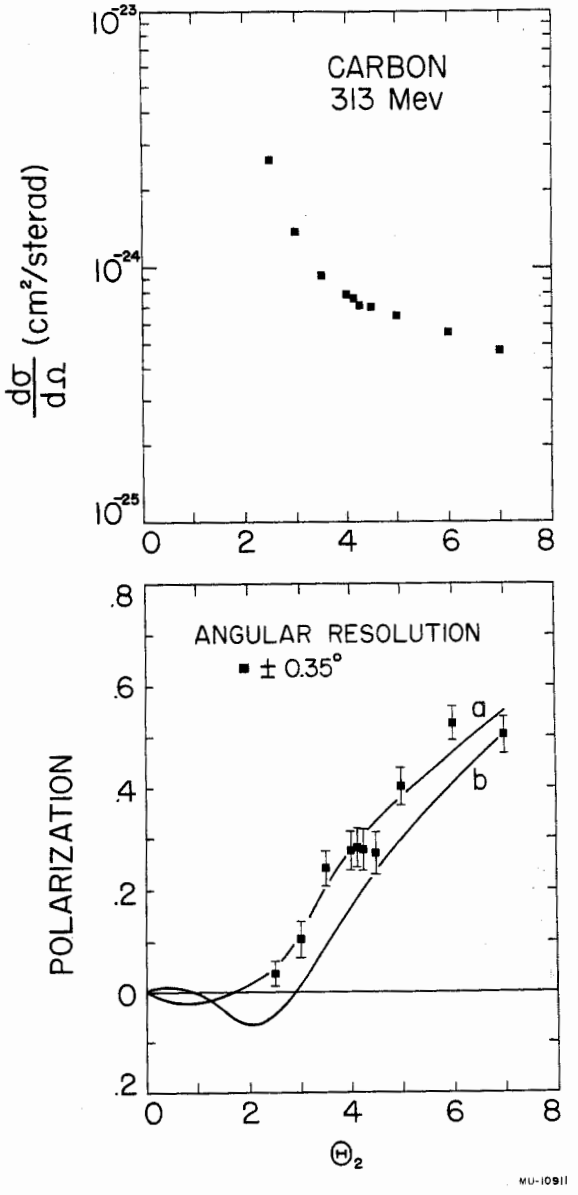

Fig. 14. Carbon small angle differential cross section and polarization at 313 Mev. The curves shown with the polarization data were obtained by Heckrotte[34] using a complex gradent type spin-orbit potential and relativistic Coulomb potential to order v/c. Curve (a) represents the choice of sign of the nuclear spin-orbit potential the same as the shell model assignment. Curve (b) corresponds to the opposite choice of sign.

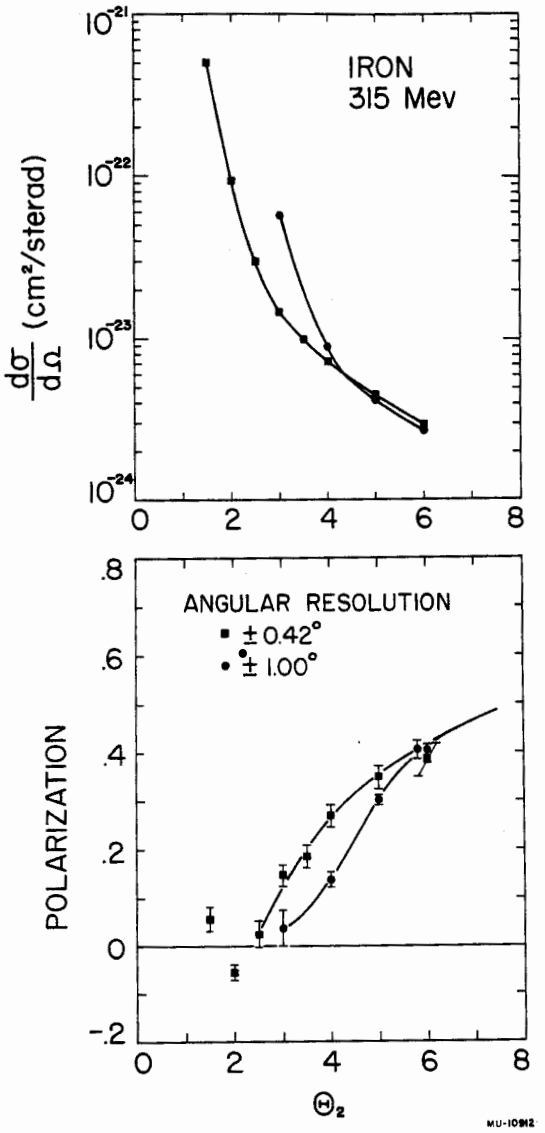

Fig. 15. Iron small angle average differential cross section and polarization at 315 Mev. The square points were obtained with an rms angular resolution of 0.42° whereas the circle points were obtained with 1.0° rms angular resolution.

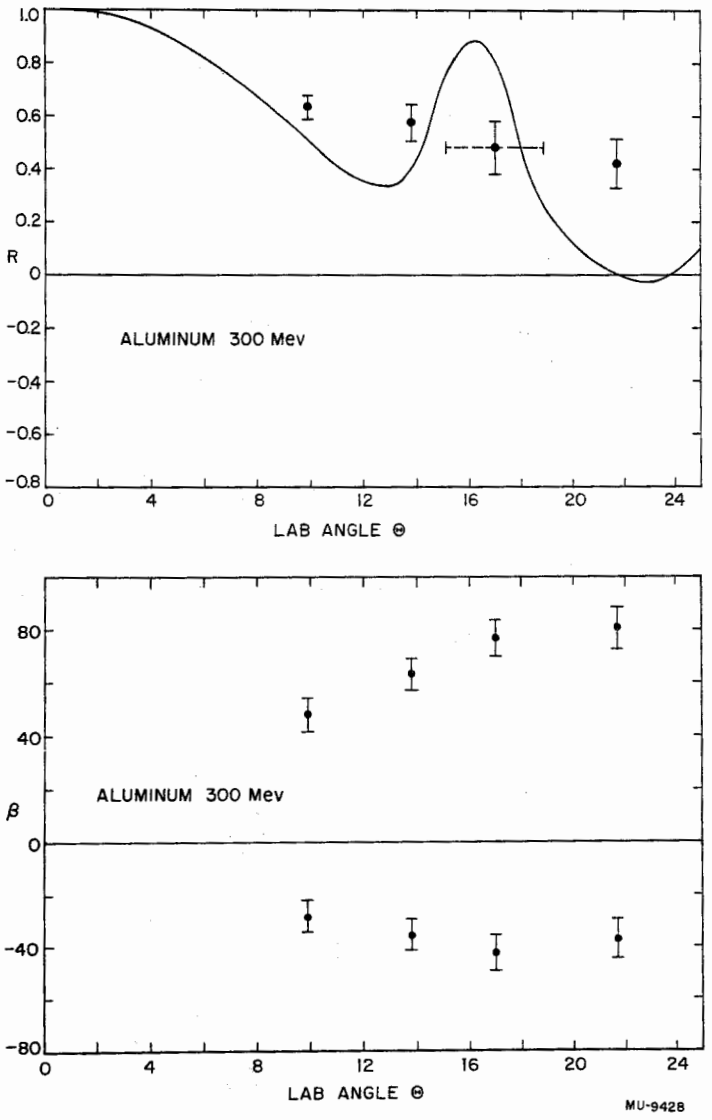

Fig. 16. Upper graph: Rotation function R vs laboratory scattering angle Θ for aluminum at an average energy of 300 Mev. The curve shown has been calculated by Heckrotte using the same potential as in Fig. 10.

Lower graph: Two possible angles of rotation β vs Θ for aluminum at 300 Mev.